iScience

CellPress
OPEN ACCESS

Article

AMPKα2 activation by an energy-independent signal ensures chromosomal stability during mitosis

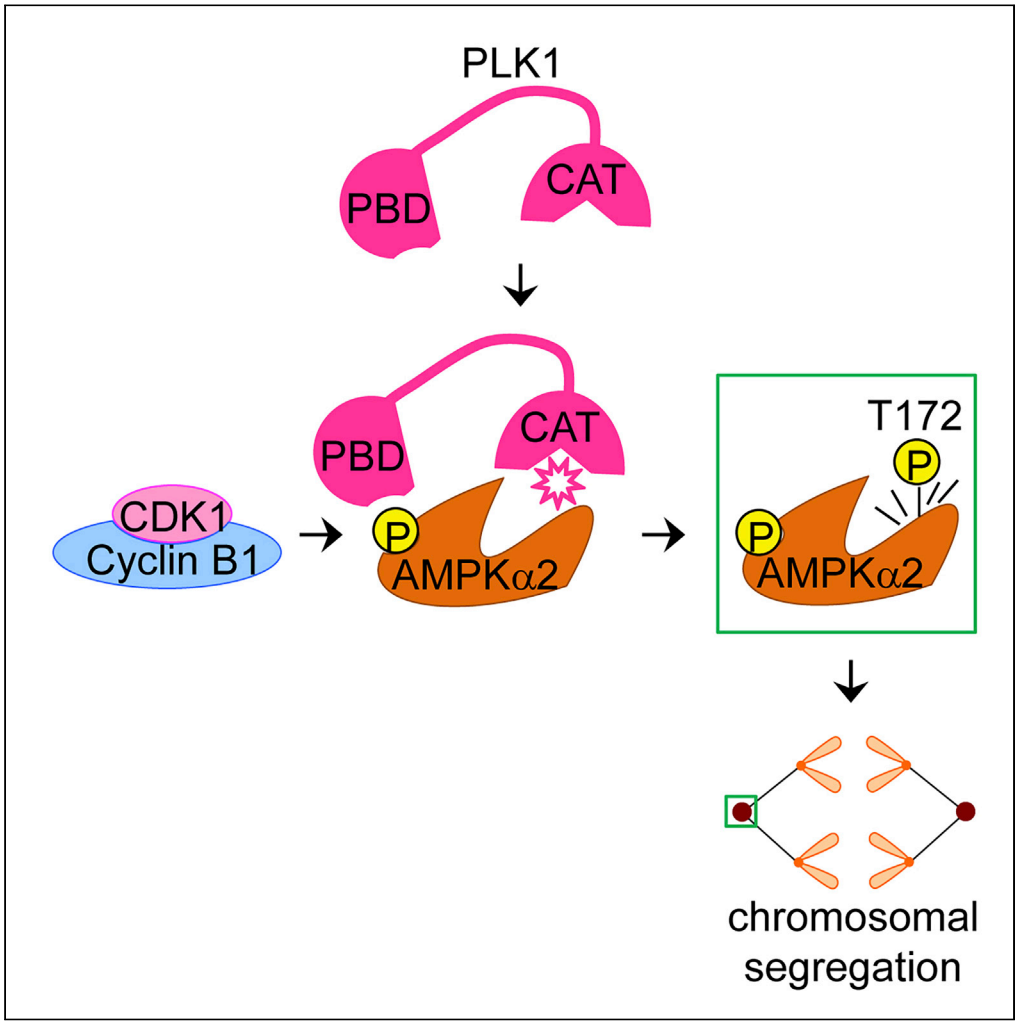

Jianlin Lu, Yuanyuan Huang, Li Zhan, ..., Wei Liu, Minerva Garcia-Barrio, Xuebiao Yao

xing1017@ustc.edu.cn (X.L.)
liuwei666@zju.edu.cn (W.L.)
minerva@med.umich.edu (M.G.-B.)
yaoxb@ustc.edu.cn (X.Y.)

Highlights

AMPKα2 is selectively activated during mitosis by CDK1 and PLK1

A conserved motif in AMPKα2 determines its interaction with and activation by PLK1

Mitotic AMPK activation contributes to maintain genomic stability in normal mitosis

Lu et al., iScience *24*, 102363
April 23, 2021
https://doi.org/10.1016/j.isci.2021.102363

iScience

CellPress
OPEN ACCESS

Article

AMPKα2 activation by an energy-independent signal ensures chromosomal stability during mitosis

Jianlin Lu,[1,2,6] Yuanyuan Huang,[1,2,6] Li Zhan,[3] Ming Wang,[1,2] Leilei Xu,[1] McKay Mullen,[1] Jianye Zang,[3] Guowei Fang,[1] Zhen Dou,[1,2] Xing Liu,[1,2,*] Wei Liu,[4,*] Minerva Garcia-Barrio,[5,*] and Xuebiao Yao[1,7,*]

SUMMARY

AMP-activated protein kinase (AMPK) senses energy status and impacts energy-consuming events by initiating metabolism regulatory signals in cells. Accumulating evidences suggest a role of AMPK in mitosis regulation, but the mechanism of mitotic AMPK activation and function remains elusive. Here we report that AMPKα2, but not AMPKα1, is sequentially phosphorylated and activated by CDK1 and PLK1, which enables AMPKα2 to accurately guide chromosome segregation in mitosis. Phosphorylation at Thr485 by activated CDK1-Cyclin B1 brings the ST-stretch of AMPKα2 to the Polo box domain of PLK1 for subsequent Thr172 phosphorylation by PLK1. Inserting of the AMPKα2 ST-stretch into AMPKα1, which lacks the ST-stretch, can correct mitotic chromosome segregation defects in AMPKα2-depleted cells. These findings uncovered a specific signaling cascade integrating sequential phosphorylation by CDK1 and PLK1 of AMPKα2 with mitosis to maintain genomic stability, thus defining an isoform-specific AMPKα2 function, which will facilitate future research on energy sensing in mitosis.

INTRODUCTION

Mitosis is an energy-consuming process essential for equal chromosome segregation. Accurate chromosome separation safeguards faithful inheritance of genetic information from a mother cell to two daughter cells (Godek et al., 2015). Mounting evidence over the last three decades has established exquisite and dynamic regulation kinase cascades such as CDK1, PLK1, Aurora A, and Aurora B in accurate cell division control (Joukov and De Nicolo, 2018).

AMPK orchestrates in a myriad of fundamental cellular processes, including autophagy, cell polarity, and mitosis (Dasgupta and Chhipa, 2016). AMPK is a heterotrimeric protein complex composed of one catalytic α subunit (α1 or α2) and two regulatory subunits, β and γ (β1 or β2, and γ1, γ2 or γ3). Combination of these multiple subunit isoforms in mammals constitutes up to 12 distinct AMPK holo-enzymes (α1β1γ1, α1β1γ2, α1β1γ3, etc.) (Lin and Hardie, 2018). It is postulated that different regulatory isoform combinations with a given catalytic subunit constitute the basis for context-dependent function of AMPK (Dasgupta and Chhipa, 2016). Under nutrient or energy starvation, activation of AMPK requires the presence of its canonical upstream kinase serine/threonine kinase 11 (LKB1) or calmodulin-dependent protein kinase kinase-β (CAMKKβ). When the cellular AMP/ATP ratio increases, excess AMP binds to the γ subunit of AMPK inducing allosteric changes of the γ subunit, which promotes Thr172 phosphorylation of AMPKα by LKB1, leading to the subsequent increase in AMPK kinase activity (Woods et al., 2003; Shaw et al., 2004). AMPK can also be activated *via* direct phosphorylation at Thr172 in response to calcium flux, through CAMKKβ (Hawley et al., 2005).

The active form AMPK localizes to the mitotic apparatus from centrosomes to spindle midzone during mitotic progression (Vazquez-Martin et al., 2009, 2011, 2012; Tripodi et al., 2018). Employing a chemical genetic screening, a study identified 28 novel substrates of AMPKα2, some of which have known roles in mitosis and cytokinesis (Banko et al., 2011). AMPK regulates the mitotic spindle orientation by phosphorylating the myosin regulatory light chain (MRLC) (Thaiparambil et al., 2012) and promotes mitotic entry by phosphorylating Golgi-Brefeldin-A-resistant GBF1, a guanine nucleotide exchange factor that is critical for Golgi disassembly during the entrance of mitosis (Mao et al., 2013; Miyamoto et al., 2008). Activation of

[1]MOE Key Laboratory for Membraneless Organelles and Cellular Dynamics, University of Science & Technology of China School of Life Sciences, Hefei 230027, China

[2]Anhui Key Laboratory for Cellular Dynamics & Chemical Biology, CAS Center for Excellence in Molecular Cell Science & Hefei National Science Center for Physical Sciences at Microscale, Hefei, Anhui 230026, China

[3]Key Laboratory of Structural Biology, Chinese Academy of Sciences, Hefei, 230027 Anhui, China

[4]Zhejiang University School of Medicine, Hangzhou, Zhejiang 310058, China

[5]University of Michigan, Ann Arbor, MI 48108, USA

[6]These authors contributed equally

[7]Lead contact

*Correspondence: xing1017@ustc.edu.cn (X.L.), liuwei666@zju.edu.cn (W.L.), minerva@med.umich.edu (M.G.-B.), yaoxb@ustc.edu.cn (X.Y.)

https://doi.org/10.1016/j.isci.2021.102363

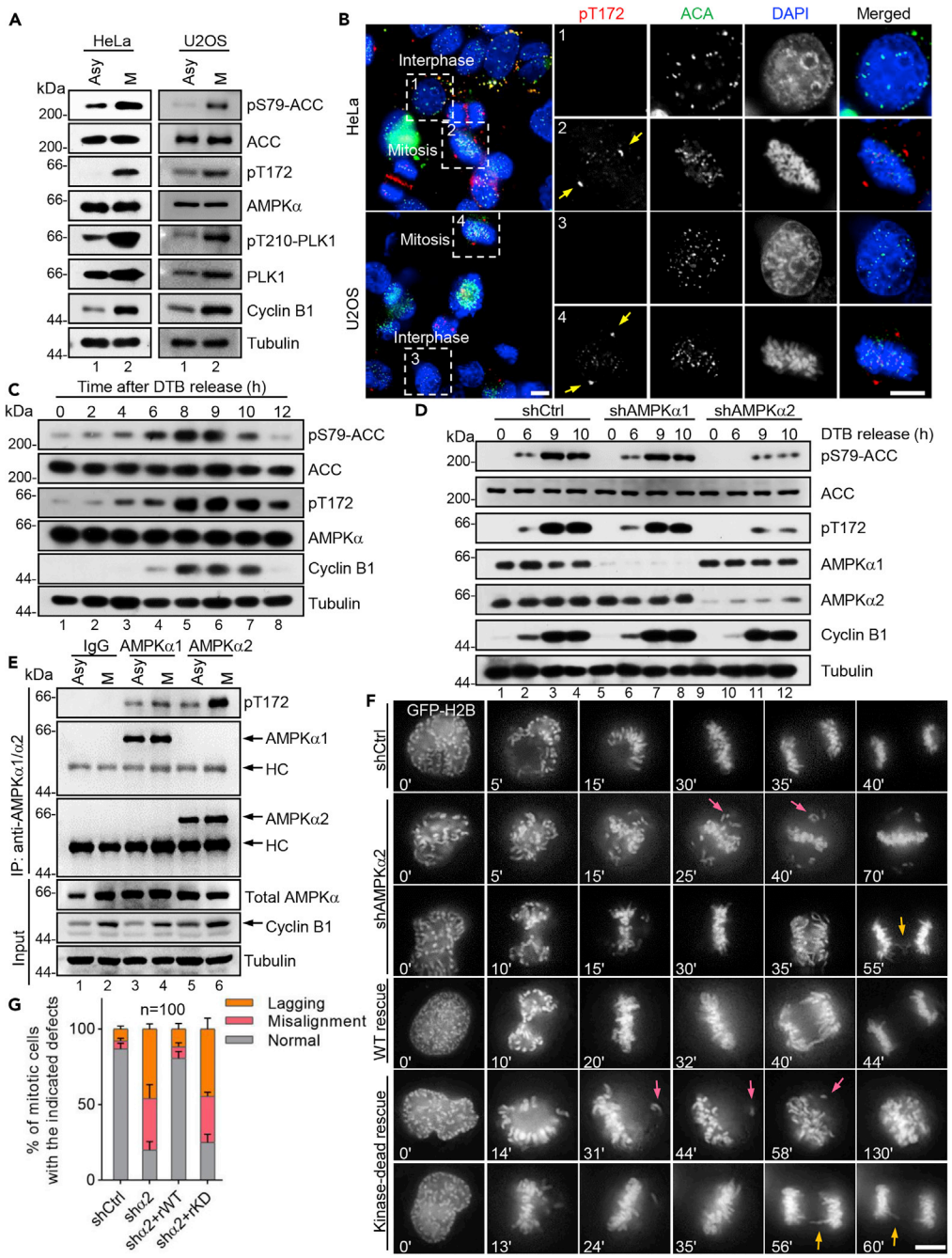

Figure 1. AMPKα2 isoform-specific activation ensures error-free chromosomal segregation

(A) The activity of AMPK in mitotic cells. HeLa and U2OS cells were synchronized in mitosis with nocodazole (100 ng/mL) block for 16 h. Samples were analyzed by western blotting with depicted antibodies. The pS79-ACC and pT172-AMPK were used as markers for AMPK activity, and pT210-PLK1, PLK1, and Cyclin B1 were used as markers for mitosis. Asy, asynchronous. M, mitotic. ACC, acetyl-CoA carboxylase (Lin and Hardie, 2018).

(B) Subcellular distribution of active form AMPK. HeLa cells (upper) and U2OS cells (lower) were stained with pT172-AMPK (red), ACA (green), and DAPI (blue) after double thymidine block (DTB, 16 h each time) release and visualized with DeltaVision microscope. ACA, anti-centromere autoimmune serum, the marker of kinetochores (Schaar et al., 1997). Thymidine, 2.5 mM. Scale bars, 10 μm.

(C) Dynamics of AMPK activity in the cell cycle. HeLa cells were synchronized at the G1/S transition by a double thymidine block/release. Samples were analyzed by western blotting with depicted antibodies. The pS79-ACC and pT172-AMPK were used as markers for AMPK activity. Thymidine, 2.5 mM.

Figure 1. *Continued*

(D) Dynamics of AMPK activity in AMPKα1-depleted or AMPKα2-depleted cells during the cell cycle. HeLa cells stably expressing shAMPKα1 or shAMPKα2 were synchronized at the G1/S transition by a double thymidine block/release. Cells were collected at the indicated time points, and samples were subjected to immunoblotting with the indicated antibodies. The pS79-ACC and pT172-AMPK were used as markers for AMPK activity.

(E) The activity of precipitated AMPKα1 or AMPKα2 in mitotic cells. AMPKα1 and AMPKα2 were separately immunoprecipitated from lysates of nocodazole-arrested HeLa cells with specific anti-AMPKα1 and anti-AMPKα2 antibodies. The precipitates were then analyzed by western blotting using the indicated antibodies. The pT172-AMPK was used as a marker for AMPK activity. Nocodazole, 100 ng/mL. Asy, asynchronous. M, mitotic. HC, heavy chain.

(F) Representative mitotic phenotypes in AMPKα2-depleted HeLa cells expressing WT AMPKα2 or AMPKα2 kinase-dead mutant (172A) shown by time-lapse microscopy, visualized with GFP-H2B. The pink arrows indicate misaligned chromosomes, and the orange arrows indicate lagging chromosomes. Numbers at the bottom left of images indicate elapsed time in minutes. Scale bar, 10 μm.

(G) Phenotypic statistics of (F). Data represent mean ± SEM. The experiment was repeated three times independently (n = 100).

AMPK in mitosis requires its upstream kinase LKB1 or CAMKKβ (Thaiparambil et al., 2012; Zhao et al., 2019; Lee et al., 2015). PLK1, an evolutionarily conserved serine/threonine kinase, is essential for mitotic processes (Macurek et al., 2008; Seki et al., 2008). Chemical inhibition of AMPK activation by PLK1 inhibitor GW843682X, together with the spatiotemporal co-localization of PLK1 and activated AMPK, suggests important role of PLK1-AMPK interaction during mitosis (Vazquez-Martin et al., 2011). As a classical mitotic kinase, PLK1 or its upstream kinase Aurora A have not yet been demonstrated to be energy sensing, challenging the view that mitotic AMPK activation is solely attributable to Thr172 phosphorylation by LKB1 elicited by ATP reduction. In fact, low energy status produces a "stop" signal that prevents cells from entering into energy-consuming mitosis (Dasgupta and Chhipa, 2016). Based on these emerging evidences, we postulate that mitotic AMPK is uncoupled from its energy sensing function in normal mitosis and may be activated by PLK1 through an alternative signaling cascade.

Here, we show that AMPK is indeed activated by PLK1 during mitosis. Neither LKB1 nor CAMKKβ are needed for normal mitotic AMPK activation. Furthermore, we found that PLK1-mediated AMPK activation requires another crucial mitotic kinase, CDK1, to prime the cascade *via* phosphorylation of the C-terminus of AMPKα2 at Thr485, which promotes the interaction between AMPK and PLK1. Interestingly, activation of AMPK in mitosis is limited to the α2 subunit. Although the α1 subunit can also be phosphorylated by CDK1 at the equivalent site corresponding to Thr485 of α2, the phosphorylated motif located on α1 is poorly recognized by PLK1. Finally, we demonstrate that activation of AMPKα2 in mitosis is essential for accurate mitotic progression and genomic integrity. Our findings reveal a distinctive sequential CDK1/PLK1-dependent and isoform-specific AMPK activation and function in mitosis.

RESULTS

AMPKα2 isoform-specific activation ensures error-free chromosomal segregation

To investigate the potential mechanism for AMPK activation in mitosis, HeLa or U2OS cells were synchronized in prometaphase with nocodazole, and cell lysates were collected and analyzed by immunoblotting. We observed dramatically increased phosphorylation of endogenous AMPK at Thr172 in the activation loop with a parallel rise in phosphorylation of its substrate, acetyl-CoA-carboxylase (ACC) at Ser79 in mitotic cells (Lin and Hardie, 2018), indicating that AMPK is active in mitosis (Figure 1A). We next determined the subcellular distribution of active AMPK by immunofluorescence with the activation loop-specific (pT172) phospho-AMPK antibody. Centrosomal localization of active AMPK was readily apparent in mitotic, but not interphase cells (Figure 1B). We also confirmed the localization of AMPK by staining HeLa cells that stably express GFP-AMPK with ACA or γ-tubulin antibody (Figures S1A and S1B). We found that AMPK shows strong centrosomal (γ-tubulin) localization, which was consistent with pT172-AMPK antibody staining. To further characterize the temporal dynamics of AMPK during cell cycle, synchronized HeLa cells were collected at various time points upon release, followed by western blot analysis. Levels of AMPK itself remained stable throughout the cell cycle, whereas the levels of both pT172 in AMPK and its substrate site, pS79 in ACC, exhibited cell-cycle-dependent dynamic changes with a peak at mitosis (Figure 1C). The consistent result was obtained by immunofluorescence staining with pT172-AMPK antibody in different mitotic stages, indicating a potential role of AMPK in mitosis (Figures S1C and S1D). This cyclic pattern of AMPK activity was reminiscent of those of Cyclin B1, PLK1, and Aurora A (Golsteyn et al., 1995; Hutterer et al., 2006; Jackman et al., 2003), supporting the proposed role of AMPK in mitosis. Furthermore,

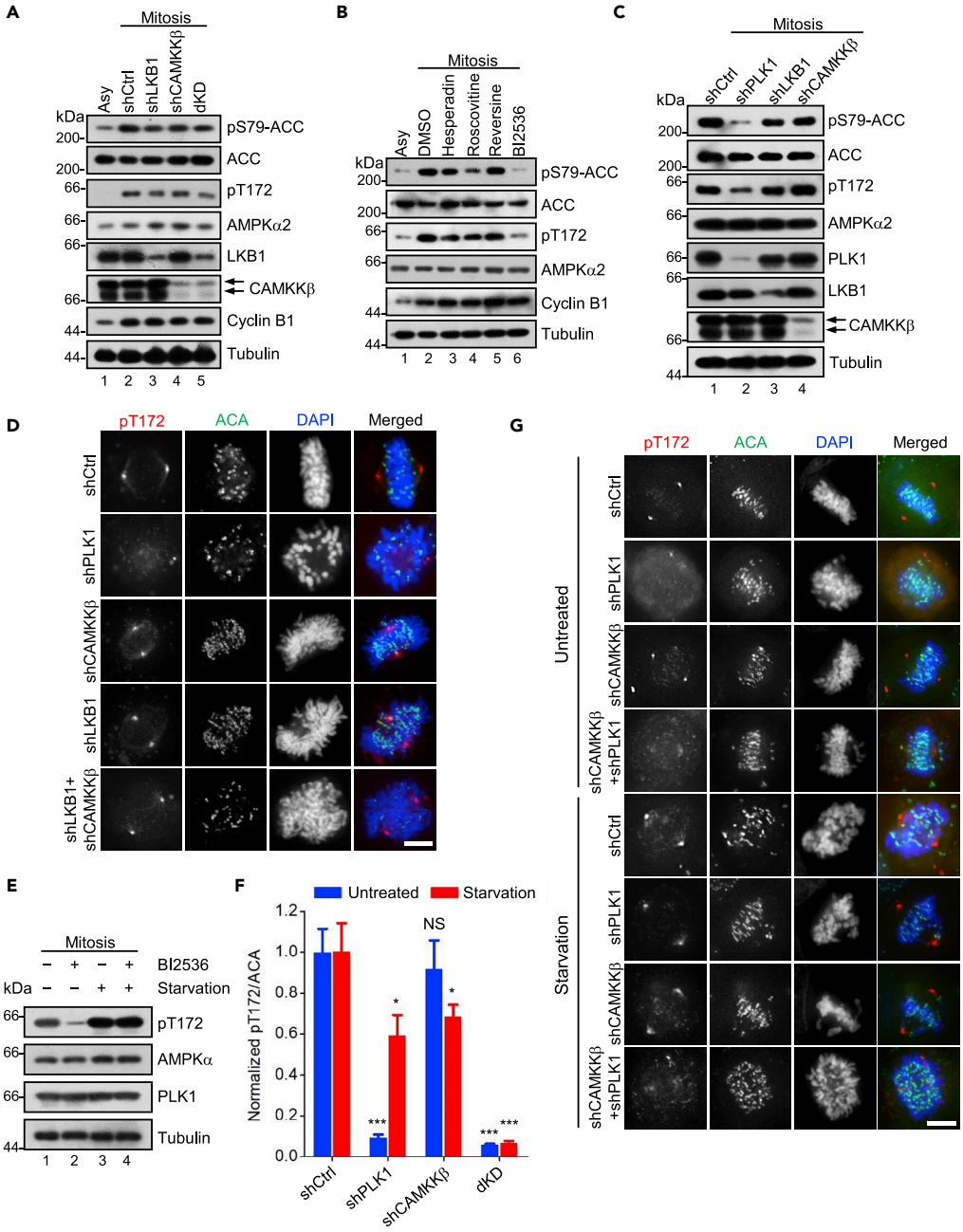

Figure 2. PLK1-dependent mitotic AMPKα2 activation is not regulated by energy stress

(A) AMPKα2 activity in LKB1-depleted, CAMKKβ-depleted, or double-depleted cells during mitosis. U2OS cells stably expressing shRNA control, LKB1 shRNA, CAMKKβ shRNA, or double knockdown (dKD) were synchronized in mitosis with nocodazole block for 16 h. The samples were subjected to immunoblotting, and AMPKα2 activity was assessed by using anti-pS79-ACC and anti-pT172-AMPK antibodies. ACC, acetyl-CoA carboxylase. Nocodazole, 100 ng/mL. Asy, asynchronous.

(B) AMPKα2 activity in mitotic cells treated with distinct kinase inhibitors. Nocodazole-arrested HeLa cells were treated with the indicated inhibitors and MG132 (10 μM) for 1 h. Cell lysates were immunoblotted with the indicated antibodies to examine AMPKα2 activity. Asynchronous cell lysates were harvested as control. Nocodazole, 100 ng/mL. Aurora B inhibitor hesperidin (25 nM), Cdk inhibitor roscovitine (50μM), Mps1 inhibitor reversine (1 μM), PLK1 inhibitor BI2536 (100 nM). Asy, asynchronous.

Figure 2. *Continued*

(C) AMPKα2 activity in PLK1-depleted, LKB1-depleted, or CAMKKβ-depleted cells during mitosis. U2OS cells stably expressing shRNA against PLK1, LKB1, or CAMKKβ were synchronized in mitosis with nocodazole block (16 h). AMPKα2 activity was analyzed by western blotting with the pS79-ACC and pT172-AMPK. Nocodazole, 100 ng/mL.

(D) Subcellular distribution of active form AMPKα2 in PLK1-depleted, LKB1-depleted, CAMKKβ-depleted, or LKB1/CAMKKβ-depleted U2OS cells during mitosis. U2OS cells stably expressing PLK1 shRNA, LKB1 shRNA, CAMKKβ-shRNA, or LKB1/CAMKKβ shRNAs were fixed, permeabilized, and stained for endogenous phospho-AMPK (red), ACA (green), and DAPI (blue) after double thymidine block (16 h each time) release. Thymidine, 2.5 mM. ACA, anti-centromere autoimmune serum, the marker of kinetochores. Scale bars, 10 μm.

(E) AMPK activity in mitotic cells treated with PLK1 inhibitor under starvation. U2OS cells were synchronized in mitosis with nocodazole block (16 h). Then, cells were treated with starvation medium (HBSS) for 1 h, in the presence of PLK1 inhibitor BI2536 and MG132. AMPK activity was analyzed by western blotting with pT172-AMPK. Nocodazole, 100 ng/mL. BI2536, 100 nM. MG132, 10 μM.

(F) Quantification of immunofluorescence intensity of pT172-AMPK as in (G). Data represent mean ± SEM. The experiment was repeated three times independently (n = 60). ***p < 0.0001. *p (shPLK1, Starvation) = 0.0194. *p (shCAMKKβ, Starvation) = 0.0228. NS (not significant) indicates p > 0.05. dKD, double knockdown (shCAMKKβ+shPLK1). Unpaired two-tailed t test for control and starvation pair in each group.

(G) Subcellular distribution of active form AMPK in PLK1-depleted and/or CAMKKβ-depleted mitotic cells under starvation. HeLa cells stably expressing PLK1 shRNA and/or CAMKKβ shRNA were synchronized in mitosis with double thymidine block (16 h each time) release and then were treated with starvation medium (HBSS) for 1 h. Cells were fixed, permeabilized, and stained for endogenous phospho-AMPK (red), ACA (green), and DAPI (blue). Thymidine, 2.5 mM. Scale bar, 10 μm.

suppression of AMPK activity with AMPK antagonist compound C in mitotic cells resulted in severe mitotic defects (Lee et al., 2020), whereas the untreated cells progressed normally (Figures S1E–S1G). This suggests that AMPK activity is essential for normal mitotic progression.

Recently, selective activation of AMPK catalytic subunits has been discovered to control specific physiological activities including fatty acid oxidation, epigenetic silencing, and endothelial proliferation (Yang et al., 2018; Lopez-Mejia et al., 2017; Wan et al., 2018). We therefore sought to ascertain whether AMPKα1 and AMPKα2 are selectively activated during mitosis. To this end, we employed a lentivirus-based gene silencing approach to specifically deplete AMPKα1 or AMPKα2 subunit. Interestingly, knockdown AMPKα2, but not AMPKα1, dramatically reduced AMPK phosphorylation at pT172, suggesting that Thr172 phosphorylation mainly occurs in AMPKα2 (Figure 1D). To confirm this unexpected finding, AMPKα2 and AMPKα1 were immunoprecipitated from asynchronous and synchronized HeLa cells, respectively and were analyzed by western blotting for phosphorylation status. As shown in Figures 1E and S1H, AMPKα2, but not AMPKα1, phosphorylation at Thr172 was dramatically increased in the mitotic immunoprecipitates. To explore the role of AMPKα2 in mitosis, we performed a knockdown/rescue experiment and observed the resulting phenotype under time-lapse microscopy (Figure 1F). Clearly, with the depletion of AMPKα2, cells exhibited a high frequency of chromosomal segregation defects, including chromosomal misalignment and lagging chromosomes. Expression of wild-type AMPKα2, but not the kinase-deficient mutant containing a T172A substitution, reversed the effect of AMPKα2 knockdown (Figures 1G, S1I, and S1J). Thus, we conclude that activated AMPKα2 is essential for accurate chromosomal segregation.

PLK1-dependent AMPKα2 activation is not regulated by energy stress

We next tested whether LKB1 or CAMKKβ were required for AMPKα2 activation in mitosis using shRNA-mediated knockdown. Surprisingly, neither CAMKKβ nor LKB1 appear to be involved in AMPKα2 activation in mitosis, as determined by the phosphorylation levels of Thr172 of AMPKα2 and of Ser79 of ACC (Figures 2A and S2A). We further examined if any other mitotic kinases regulate AMPKα2 activity using chemical inhibition. As shown in Figure 2B and Figure S2B, BI2536, a selective inhibitor of PLK1 (Steegmaier et al., 2007), almost completely suppressed AMPKα2 activity judged by pT172-AMPK and pS79-ACC without affecting the levels of AMPKα2 protein. In addition, the Cdk inhibitor roscovitine attenuated AMPKα2 activity, albeit mild compared with that of BI2536 (Figures 2B and S2B). We further verified the impact of PLK1 on AMPKα2 activation by using lentivirus-based PLK1 gene silencing in cells. Consistent with the results observed in Figures 2C and S2C, the centrosomal signal of pT172-AMPKα2, rather than AMPKα2 itself (Figure S2D), was abolished in PLK1 shRNA-treated cells (Figures 2D, S2E, and S2F). Collectively, these correlative studies suggest that PLK1 is responsible for AMPKα2 activation in mitosis.

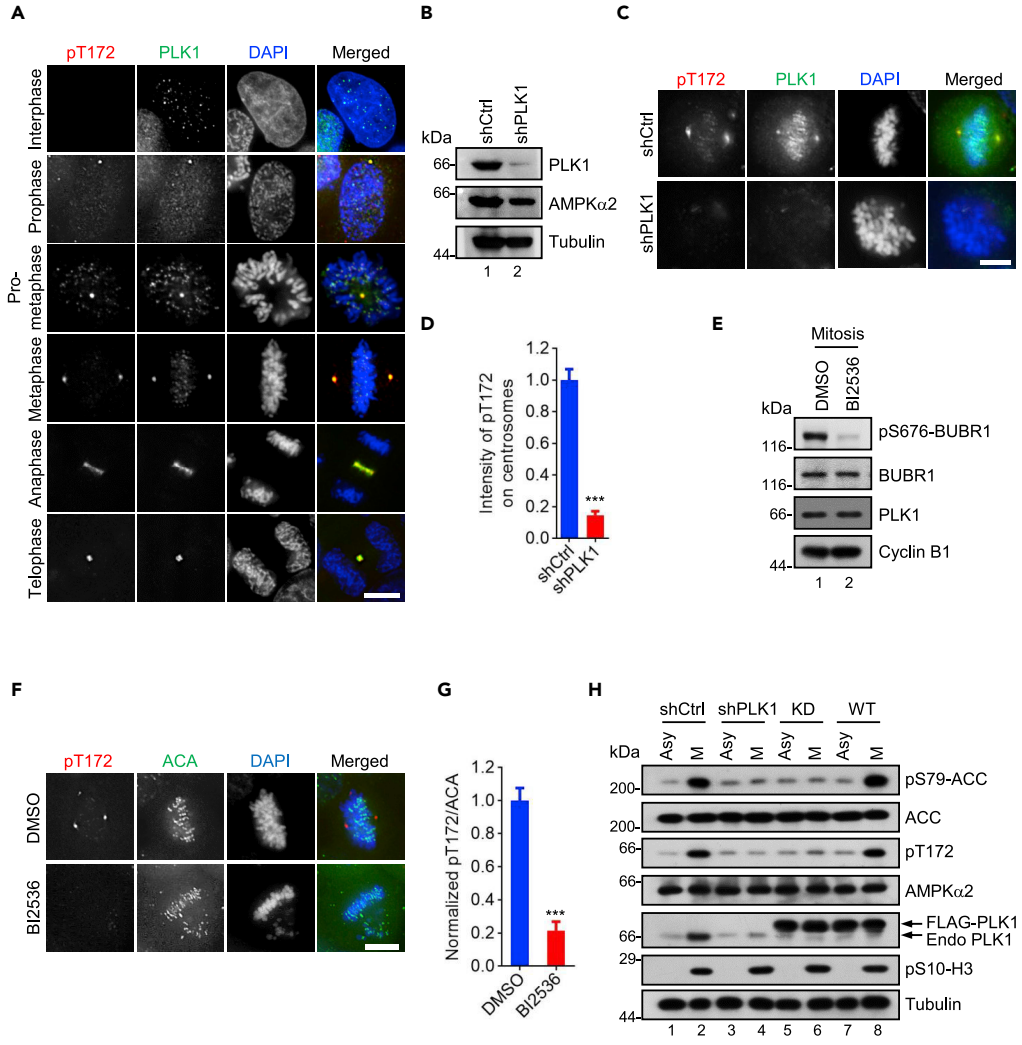

Figure 3. PLK1 regulates AMPKα2 activity

(A) Co-localization of PLK1 and active form AMPKα2 in HeLa cells from different mitotic stages. HeLa cells were treated with double thymidine block (16 h each time) followed by releasing for 8 h. Cells were fixed, permeabilized, and stained for endogenous phospho-AMPK (red), PLK1 (green), and DAPI (blue). Thymidine, 2.5 mM. Scale bars, 10 μm.

(B) Protein level of AMPKα2 in PLK1-depleted cells. HeLa cells stably expressing PLK1 shRNA were collected and cell lysates were analyzed by western blotting using an anti-AMPKα2 antibody.

(C) Immunostaining of active form AMPKα2 in PLK1-depleted cells. HeLa cells stably expressing PLK1 shRNA were treated with double thymidine block (16 h each time) followed by releasing for 8 h. Cells were fixed and stained for endogenous phospho-AMPK (red), PLK1 (green), and DAPI (blue). Scale bar, 10 μm.

(D) Quantification of immunofluorescence intensity in (C). Data represent mean ± SEM. The experiment was repeated three times independently (n = 60). Statistical significance was determined by unpaired two-tailed t test. ***p < 0.0001. The average +/− SEM of each pane was 1.000 ± 0.06826, 0.1464 ± 0.02430.

(E) Assessment of the inhibitory effect of BI2536 on PLK1 activity. HeLa cells were synchronized in mitosis with nocodazole block (16 h). Then, cells were treated with BI2536 for 1 h. PLK1 activity was analyzed by western blotting with pS676-BUBR1. The pS676-BUBR1 was used as a marker for PLK1 activity. Nocodazole, 100 ng/mL. BI2536, 100 nM.

(F) Immunostaining of active form AMPKα2 in HeLa cells treated with PLK1 inhibitor BI2536. HeLa cells were treated with double thymidine block (16 h each time) followed by releasing for 8 h and then were treated with BI2536 for 1 h. Cells were fixed and stained for endogenous phospho-AMPK (red), ACA (green), and DAPI (blue). ACA, anti-centromere autoimmune serum, the marker of kinetochores. Scale bar, 10 μm.

(G) Quantification of immunofluorescence intensity in (F). Data represent mean ± SEM. The experiment was repeated three times independently (n = 60). Statistical significance was determined by unpaired two-tailed t test. ***p < 0.0001. The average +/− SEM of each pane was 1.000 ± 0.07472, 0.2137 ± 0.05483.

Figure 3. *Continued*
(H) AMPKα2 activity in PLK1-depleted HeLa cells overexpressing WT PLK1 or the kinase-dead (KD) mutant. HeLa cells stably expressing PLK1 shRNA were infected with lentivirus-based particles overexpressing wild-type PLK1 or kinase-dead mutant (PLK1 K82R). Then, cells were treated with nocodazole for 16 h and were subjected to immunoblotting with the indicated antibodies. The pS79-ACC and pT172-AMPK were used as markers for AMPKα2 activity. The pS10-H3 was used as a marker for mitosis. ACC, acetyl-CoA carboxylase. Endo PLK1, endogenous PLK1. Asy, asynchronous. M, mitosis. Nocodazole, 100 ng/mL.

Our data demonstrated that PLK1 regulates AMPKα2 activation at the centrosomes during mitosis. To examine if nutrient starvation would regulate AMPK activity in mitosis, we subjected nocodazole-synchronized U2OS cells to nutrient starvation followed by western blot analysis. As shown in Figures 2E and S2G, chemical inhibition of PLK1 dramatically reduced AMPK activity in normal mitotic cells judged by pT172 abundance but not in nutrient starved cells in mitosis, suggesting that AMPK activity in mitotic cells could be contextually regulated by PLK1-dependent and PLK1-independent pathways. To further characterize if centrosomal AMPK activity is a function of PLK1 during mitotic starvation, synchronized HeLa cells were then fixed and examined for phosphorylation of AMPK in cells at metaphase. As shown in the studies above, suppression of PLK1 prevented AMPK activation at the centrosomes of control cells (Figures 2F, 2G, and S2H). However, in the starvation group, suppression of PLK1 did not alter AMPK activity at the centrosomes. The AMPK activation by nutrient starvation in mitosis was eliminated only when both CAMKKβ and PLK1 were knocked down (Figures 2F, 2G, and S2H). Thus, these data indicate that PLK1 is responsible for AMPKα2 activation during regular mitotic processes, whereas LKB1 or CAMKKβ participates in stress response in nutrient-deficient mitosis.

PLK1 regulates mitotic AMPKα2 activity

To further examine the role of PLK1 in regulating AMPKα2, we first characterized the subcellular distribution of PLK1 relative to activated AMPKα2 during cell division. Several studies demonstrated this co-distribution of PLK1 with activated AMPK at each stage of mitosis (Vazquez-Martin et al., 2011). Our immunofluorescence study experiments demonstrated that PLK1 and activated AMPKα2 are co-localized to the centrosomes in mitotic cells (Figure 3A), thus assigning a distinct role for AMPKα2 in mitosis. When PLK1 was knocked down, the level of activated AMPKα2 was dramatically reduced (Figures 3B–3D), indicating the activated AMPKα2 is a function of PLK1 in mitosis. And pT172 signal was abolished in cells depleted of AMPKα2, suggesting the specificity of pT172-AMPK antibody (Figure S3A). Consistent with this notion, chemical inhibition of PLK1 activity by BI2536 also abolished AMPK activation during mitosis (Figures 3E–3G, S3B, and S3C). Our western blotting analyses show that BI2536 inhibits PLK1 activity without alteration of PLK1 protein level (Figure 3E). These results suggest that PLK1 kinase activity, rather than the protein itself, is necessary for AMPKα2 activation. Indeed, exogenous expression of wild-type PLK1 in HeLa cells deficient in endogenous PLK1 restored AMPK activity in mitosis, whereas expression of a kinase-dead mutant of PLK1 failed to restore AMPK activity judged by western blotting analyses of pT172-AMPK and pS79-ACC (Figures 3H and S3D). Thus, we conclude that PLK1 kinase activity is essential for mitotic AMPKα2 activation.

PLK1 binds specifically to AMPKα2 *via* the PBD domain

To understand the mechanisms underlying PLK1-elicited AMPKα2 activation in mitosis, we examined the interaction between PLK1 and AMPKα2. As shown in Figures 4A and S4A, endogenous PLK1 was co-precipitated with AMPKα2, but not AMPKα1, which is consistent with the finding above that AMPKα1 is not activated during mitosis. Early study claimed that PLK1 is co-localized with activated AMPK at each stage of mitosis (Vazquez-Martin et al., 2011), and our experiments demonstrate the co-localization of PLK1 and AMPKα2 at centrosomes during mitosis by stable cell line and PLK1 antibody (Figure 4B). Interestingly, we found that PLK1 disappears from centrosomes earlier than AMPKα2 in anaphase (Figure 4B). In addition, as shown in Figure 3A, pT172-AMPK signal was abolished in anaphase, confirming the role of PLK1 in regulating AMPK activity during mitosis. To further characterize PLK1-AMPKα2 interaction and pinpoint the binding interface between the AMPKα2 and PLK1 proteins, FLAG-PLK1 and various GFP-AMPKα2 deletion mutants were constructed and were co-transfected with FLAG-PLK1 into HEK293T cells. Our experiments demonstrated that the C-terminus of AMPKα2 was required for its interaction with PLK1 (Figures 4C, S4B, and S4C). Because PLK1 possesses several functionally distinct domains, we next examined the region of PLK1 which mediates its binding to AMPKα2. To this end, different recombinant GST-PLK1 proteins bound to glutathione agarose beads were used as affinity

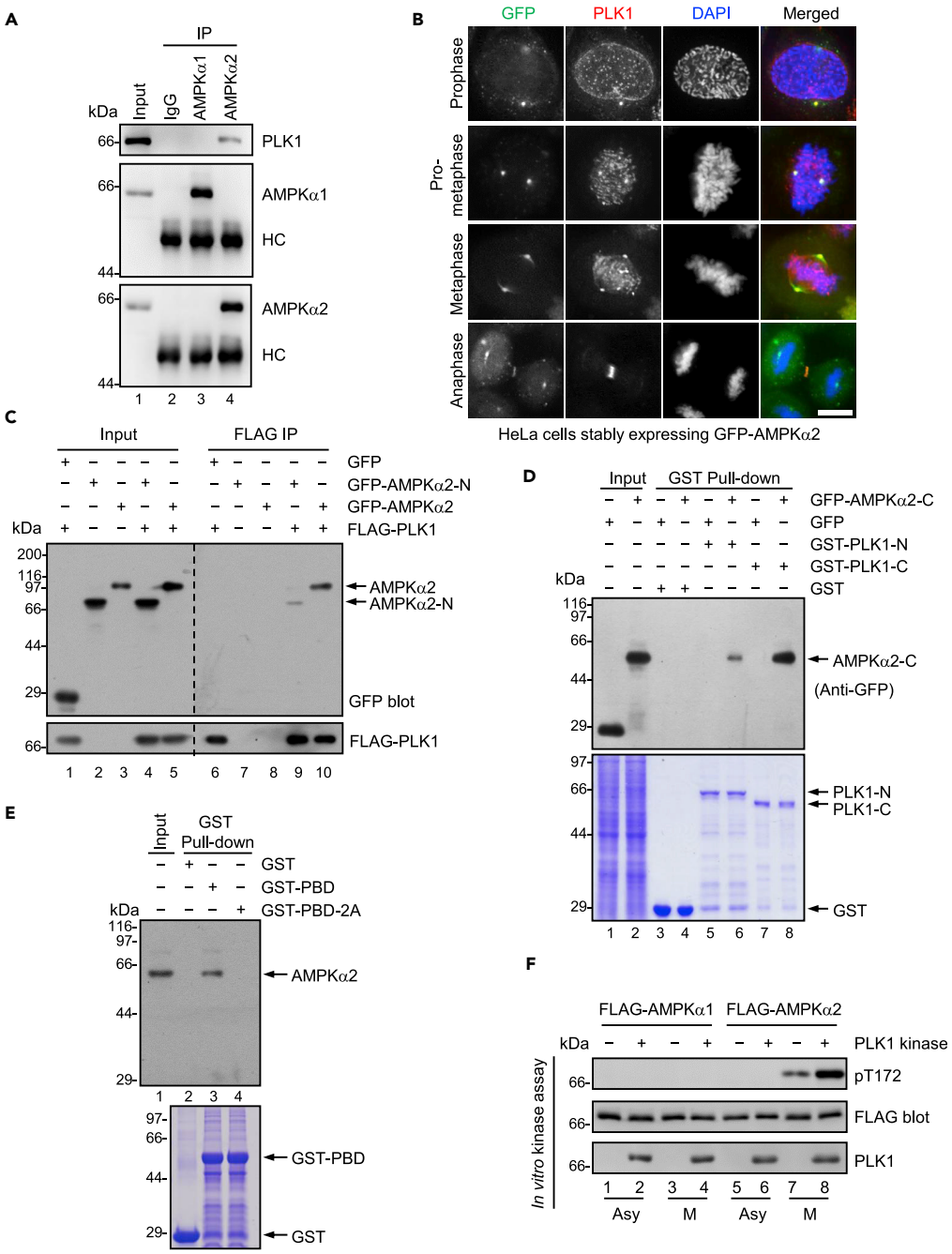

Figure 4. PLK1 binds specifically to AMPKα2 via the PBD domain

(A) Interaction of endogenous PLK1 with AMPKα1 or AMPKα2 in U2OS cells by immunoprecipitation with AMPKα1 or AMPKα2 antibody, respectively followed by western blotting with the anti-PLK1 antibody. HC, heavy chain.

(B) Co-localization of AMPKα2 and PLK1 in HeLa cells from different mitotic stages. HeLa cells stably expressing GFP-AMPKα2 were treated with double thymidine block (16 h each time) followed by releasing for 8 h and then were fixed and stained for endogenous PLK1 (red) and DAPI (blue). Thymidine, 2.5 mM. Scale bar, 10 μm.

(C) Co-immunoprecipitation of GFP-AMPKα2 or GFP-AMPKα2-N with FLAG-PLK1. FLAG-PLK1 was co-transfected with GFP-AMPKα2 or GFP-AMPKα2-N (N-terminus, amino acids 1-376) in HEK293T cells. Immunoprecipitation was carried out with anti-FLAG, and the precipitates were immunoblotted with anti-GFP.

(D) Pull-down assay of recombinant GST-PLK1-N or recombinant GST-PLK1-C with GFP-AMPKα2-C. Lysates of HEK293T cells transiently expressing GFP-AMPKα2-C (C-terminus, amino acids 377-552) were incubated with bacterially expressed

Figure 4. *Continued*

and purified GST-PLK1-N (N-terminus, amino acids 1-326) or GST-PLK1-C (C-terminus, amino acids 327-603), and a pull-down assay was performed using anti-GST. The bound AMPKα2-C was detected with anti-GFP.

(E) Pull-down assay of endogenous AMPKα2 in treated HeLa cells with recombinant GST-PBD or GST-PBD-2A mutant. Purified GST-PBD or GST-PBD-2A (H538A/K540A) was incubated with lysates of nocodazole-arrested (16 h) HeLa cells, and a pull-down assay was performed using anti-GST. The bound AMPKα2 was detected with the anti-AMPKα2 antibody. Nocodazole, 100 ng/mL.

(F) *In vitro* kinase assays using recombinant PLK1 kinase and stably expressing FLAG-tagged AMPKα1 or AMPKα2 immunoprecipitated from nocodazole-arrested HeLa cells. Then each of the purified proteins was incubated with recombinant PLK1 kinase, and an *in vitro* kinase assay was performed. The phosphorylation levels of AMPKα1 and AMPKα2 were detected with the anti-pT172-AMPK antibody. Asy, asynchronous. M, mitosis.

matrix to bind GFP-AMPKα2-C from HEK293T cell lysates. As shown in Figure 4D, the C-terminus of PLK1 retained GFP-AMPKα2-C, indicating that the polo-box binding domain (PBD) mediates the interaction of PLK1 and GFP-AMPKα2. To determine their physical interaction, bacterially expressed recombinant GST-PBD or GST-PBD-2A mutant (H538A/K540A; negative control) (Garcia-Alvarez et al., 2007) were incubated with mitotic HeLa cell lysates. GST pull-down analyses showed that AMPKα2 interacts with PBD but not PBD-2A mutant (Figure 4E). Furthermore, we immunoisolated FLAG-AMPKα2 protein from stably expressed HeLa cells and performed *in vitro* kinase assays. Mitotic AMPKα2 exhibits a basal phosphorylation at Thr172 without addition of PLK1. However, the phosphorylation at Thr172 was markedly augmented in the presence of addition of PLK1. In parallel experiment, we failed to detect apparent phosphorylation signals of AMPKα2 from asynchronous cell lysates, AMPKα1 from mitotic cell lysates, or AMPKα1 from asynchronous cell lysates, with or without PLK1 kinase (Figure 4F). Thus, we conclude that PLK1 interacts with the C-terminal region of AMPKα2 via its PBD and selectively phosphorylates AMPKα2 isolated from mitotic but not interphase cells.

Activation of AMPKα2 by PLK1 depends on Thr485 phosphorylation

The PBD of PLK1 is a signaling module that recognizes a conserved consensus motif S-(pT/pS)-(P/X) on its effectors, and CDK1 priming phosphorylation is essential for PBD domain binding (Elia et al., 2003a, 2003b). Given the suppression of pT172 level by the CDK inhibitor roscovitine (Figures 2B and S2B), we hypothesized that CDK1 may phosphorylate AMPKα2 at a priming site (or sites), which promotes the interaction between PBD and AMPKα2 for optimal activation of AMPKα2 by PLK1. Sequence alignment analyses revealed that AMPKα2 in multicellular organisms contained potential phosphorylation sites (Thr85, Ser345, and Thr485) for CDK1, and these sites are consistent with the PLK1 docking motif (Figure 5A). Recent work suggested that CDK1 can phosphorylate multiple subunits of AMPK (Stauffer et al., 2019). Thus, we proposed that AMPKα2 was phosphorylated by CDK1 before PLK1-mediated phosphorylation at Thr172. To test this hypothesis, we first examined if AMPKα2 interacts with the CDK1-Cyclin B1 complex. As shown in Figure S5A, immunoprecipitation of FLAG-AMPKα2 from HeLa cell lysates co-precipitated CDK1-Cyclin B1. Further, utilizing recombinant MBP-AMPKα2 purified from *Escherichia coli* as a substrate and pCDK-sub, an antibody that specifically recognizes the phosphorylated substrates of CDK kinase (Whalley et al., 2015), *in vitro* kinase assay indicated that CDK1 was able to phosphorylate AMPKα2 and the phosphorylation level was significantly reduced in the presence of CDK1 inhibitor RO-3306 (Figure S5B). To pinpoint the phosphorylated sites in AMPKα2, we subjected purified AMPKα2 phosphorylated by CDK1-Cyclin B1 to mass spectrometric analysis and identified three sites: Ser345, Ser377, and Thr485 (Figures S5C and S5E). To confirm that these three identified sites are substrates of CDK1, we created AMPKα2 mutants by replacing the three residues with alanine and performed *in vitro* kinase assays. Direct phosphorylation of AMPKα2 by CDK1 was detected with ^{32}P-labeled ATP and pCDK-sub. However, single residue replacement moderately reduced AMPKα2 phosphorylation, and triple residue replacement eliminated AMPKα2 phosphorylation, confirming that they are the major CDK1 phosphorylation sites on AMPKα2 (Figures S5F and S5G).

To further test whether these sites are all responsible for AMPK activation, we generated a series of AMPKα2 mutants in which the three phosphorylated sites were individually mutated to alanine. To our surprise, FLAG-AMPKα2 T485A mutant isolated from mitotic cells contained minimal level of phospho-Thr172, whereas the other two FLAG-AMPKα2 site-specific mutants (S345A or S377A) exhibited no alteration of the pT172 level (Figures 5B and S5H), suggesting that Thr485 phosphorylation was required as priming for mitotic PLK1-dependent AMPKα2 activation. To assess the spatiotemporal dynamics of CDK1-elicited phosphorylation of AMPKα2 and study its relevance in mitosis, we generated a phospho-Thr485-specific

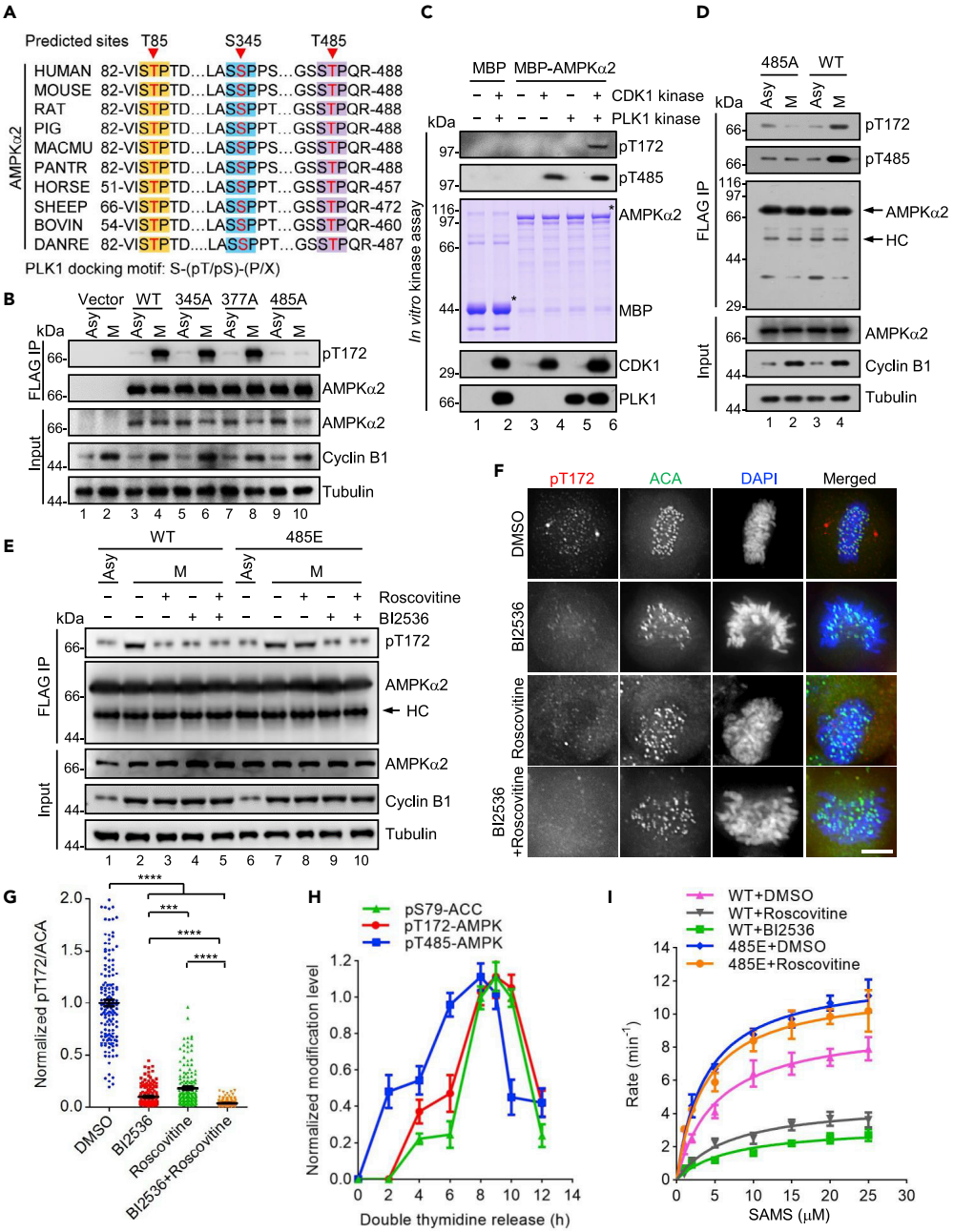

Figure 5. Phosphorylation and activation of AMPKα2 by PLK1 depends on T485 priming phosphorylation

(A) Cluster alignment of three conserved sites in AMPKα2 matching the optimal CDK1 substrate motif.

(B) The activity of FLAG-tagged AMPKα2 mutants immunopurified from transfected mitotic cells. U2OS cells transfected with FLAG-AMPKα2, FLAG-AMPKα2-345A, FLAG-AMPKα2-377A, or FLAG-AMPKα2-485A were synchronized in mitosis with nocodazole block. Then each of the exogenous AMPKα2 mutants was immunoprecipitated with anti-FLAG, and AMPKα2 activity was analyzed by western blotting using an anti-pT172-AMPK antibody. Nocodazole, 100 ng/mL. Asy, asynchronous. M, mitotic.

(C) *In vitro* kinase assays using recombinant MBP-AMPKα2, in the presence of CDK1-Cyclin B1 kinase, or PLK1 kinase, or with CDK1-Cyclin B1, added to the kinase assay first followed by PLK1 addition. Samples were subjected to immunoblotting with the indicated antibodies and CBB staining.

(D) The phosphorylation levels of Thr485 and Thr172 of AMPKα2 or AMPKα2-485A mutant immunopurified from mitotic cells. U2OS cells stably expressing FLAG-tagged AMPKα2 or AMPKα2-485A mutant were synchronized in mitosis with nocodazole block. The exogenous AMPKα2 or AMPKα2-485A mutant was immunoprecipitated with anti-FLAG, and the

Figure 5. *Continued*

phosphorylation levels were analyzed by western blotting using anti-pT172-AMPK antibody and anti-pT485-AMPK antibody. Nocodazole, 100 ng/mL. Asy, asynchronous. M, mitotic. HC, heavy chain.

(E) The activity of AMPKα2 or AMPKα2-485E mutant immunopurified from mitotic cells treated with CDK1 inhibitor and/or PLK1 inhibitor. U2OS cells stably expressing FLAG-tagged AMPKα2 or AMPKα2-485E mutant were synchronized in mitosis with nocodazole block. Then the cells were treated with Cdk inhibitor roscovitine and/or PLK1 inhibitor BI2536 for 1 h, in the presence of MG132. The exogenous AMPKα2 or AMPKα2-485E mutant was immunoprecipitated with anti-FLAG, and the activity was analyzed by western blotting using an anti-pT172-AMPK antibody. Asy, asynchronous. M, mitotic. HC, heavy chain. Roscovitine, 50 μM. BI2536, 100 nM. MG132, 10 μM.

(F) Immunostaining of active form AMPKα2 in HeLa cells treated with PLK1 inhibitor BI2536 and/or Cdk inhibitor roscovitine. HeLa cells were treated with double thymidine block (16 h each time) followed by releasing for 8 h and then were treated with PLK1 inhibitor BI2536 and/or Cdk inhibitor roscovitine for 1 h before harvest. Cells were fixed and stained for endogenous phospho-AMPK (red), ACA (green), and DAPI (blue). Thymidine, 2.5 mM. BI2536, 100 nM. Roscovitine, 50 μM. Scale bar, 10 μm.

(G) Quantification of fluorescence intensity of pT172 in (F). The experiment was repeated three times independently. DMSO, n = 50; BI2536, n = 60; Roscovitine, n = 55; BI2536 + Roscovitine, n = 58. Data represent mean ± SEM. Non-parametric Kruskal-Wallis test followed by Dunn's multiple comparisons test ****$p < 0.0001$; ***$p < 0.0001$. The average +/− SEM of each pane was 1.001 ± 0.03192, 0.09990 ± 0.006405, 0.1804 ± 0.01396, 0.03520 ± 0.002271.

(H) Temporal profile of Cyclin B accumulation, Thr172-AMPK phosphorylation, Thr485-AMPK phosphorylation, and Ser79-ACC phosphorylation. HeLa cells were synchronized at the G1/S boundary by double thymidine block (16 h each time) and released to the indicated time points. Samples were analyzed with depicted antibodies. Data represent mean ± SEM from densitometry of western blots. The experiment was repeated three times independently. Thymidine, 2.5 mM.

(I) HeLa cells stably expressing FLAG-tagged AMPKα2 or AMPKα2-485E mutant were synchronized in mitosis with nocodazole block (16 h), then cells were treated with Cdk inhibitor roscovitine or PLK1 inhibitor BI2536 for 1 h before collection. The exogenous AMPKα2 or AMPKα2-485E mutant was immunoprecipitated with anti-FLAG and was eluted with FLAG peptide. Kinetics curves of AMPKα2 or AMPKα2-485E kinase activity were measured at various concentrations of SAMS (AMPK substrate peptide) in the indicated conditions. The background fluorescence was determined by measuring the fluorescence intensity in the absence of substrate and subtracted from the experiments. Data represent mean ± SEM. Nocodazole, 100 ng/mL. BI2536, 100 nM. Roscovitine, 50 μM.

antibody (pT485) that specifically recognized phosphorylated AMPKα2. As shown in Figure S5I, the levels of pT485 were increased by nocodazole treatment but diminished soon after inhibition with the CDK1 inhibitor roscovitine. Then, we designed an *in vitro* kinase assay using purified MBP-AMPKα2 as substrate, in the presence of CDK1 kinase, or PLK1 kinase, or both. Incubation of AMPKα2 with the two kinases, rather than PLK1 or CDK1 alone, promoted the phosphorylation of Thr172 (Figure 5C). To further delineate the function of CDK1 in AMPKα2 activation, U2OS cells expressing FLAG-AMPKα2 and various mutants were synchronized in mitosis with nocodazole, and lysates were subjected to immunoprecipitation. Western blot analysis for pT172 level revealed that FLAG-AMPKα2 (T485A) isolated from mitotic cells exhibited little phosphorylation when compared with the WT allele, indicating impaired activation (Figure 5D). In contrast, AMPKα2 (T485E), mimicking CDK1 phosphorylation at Thr485 and showing the same localization with wild type (Figure S5J), isolated from mitotic cells exhibited comparable level of phosphorylation at Thr172 as wild type (Figure 5E), consistent with the importance of priming by CDK1-dependent phosphorylation at Thr485 for AMPKα2 activation. Accordingly, treatment of mitotic cells with the CDK1 inhibitor roscovitine or PLK1 inhibitor BI2536 prevented the enhanced pT172-AMPK signal observed in wild-type FLAG-AMPKα2 in mitosis. In contrast, Thr172 phosphorylation of FLAG-AMPKα2 (T485E) was not influenced by roscovitine but was inhibited by BI2536 (Figure 5E). Furthermore, immunofluorescence assay showed that inhibition of either CDK1 or PLK1 attenuated the pT172 signal at the centrosomes, and simultaneous inhibition of both PLK1 and CDK1 abolished AMPKα2 activation at the centrosomes with an additive effect (Figures 5F and 5G). We next tested the cell-cycle dynamics of pT485 relative to pT172 during mitosis. Lysates of synchronized HeLa cells at the indicated time points after release from the G1/S phase were collected for immunoblotting analysis. As shown in Figure S5K and plotted in 5H, the temporal dynamics of pT485 was similar to that of Cyclin B1, consistent with the notion that Thr485 of AMPKα2 was regulated by CDK1-Cyclin B1. Furthermore, pT172-AMPK and pS79-ACC (targeting site of AMPK on ACC) levels were similar to those of pT485 but with a brief lag, suggesting that the AMPKα2 activity might be regulated by CDK1-elicited Thr485 phosphorylation. We also incubated the SAMS peptide (substrate of AMPK) (Sullivan et al., 1994; Kishimoto et al., 2006) with either FLAG-AMPKα2 WT or the T485E and T485A mutants immunoprecipitated from mitotic cells, for *in vitro* kinase assays and enzymatic characterization. CDK1-mediated Thr485 phosphorylation robustly stimulated AMPKα2 activity (Figures 5I and S5L). These results show that CDK1-mediated phosphorylation of Thr485 promotes the subsequent phosphorylation of Thr172 by PLK1, leading to the activation of AMPKα2 during mitosis.

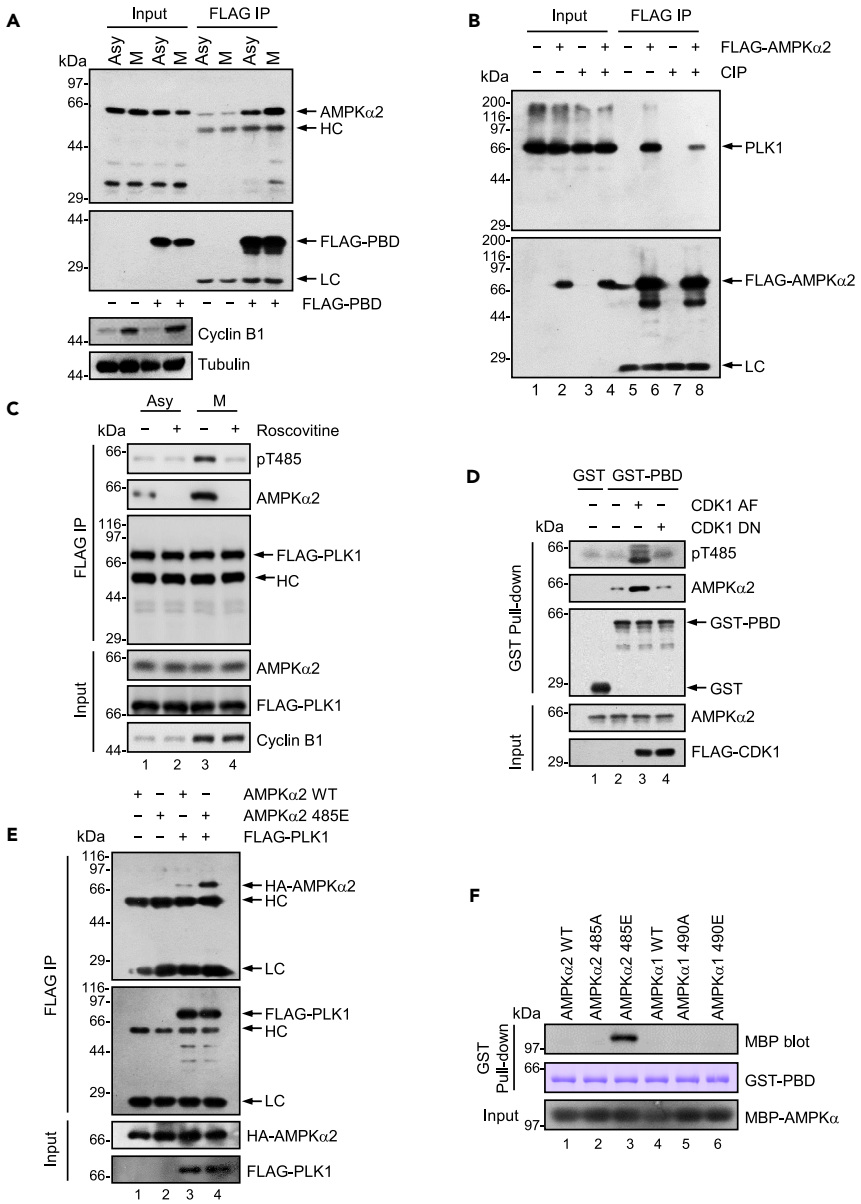

Figure 6. T485 phosphorylation promotes the binding of PLK1 to AMPKα2

(A) Co-immunoprecipitation of endogenous AMPKα2 with the PBD domain of PLK1 in mitotic cells. U2OS cells transfected with FLAG-PBD were synchronized in mitosis with nocodazole (16 h) block. FLAG-PBD was immunoprecipitated with anti-FLAG, and the bound AMPKα2 was detected with anti-AMPKα2. Nocodazole, 100 ng/mL. Asy, asynchronous. M, mitotic. HC, heavy chain. LC, light chain.

(B) Co-immunoprecipitation of endogenous PLK1 with FLAG-AMPKα2 in mitotic cells treated with phosphatase. U2OS cells transiently expressing FLAG-AMPKα2 were synchronized in mitosis with nocodazole block (16 h). Cell lysates were incubated with calf intestinal alkaline phosphatase (CIP) at 37°C for 1 h, and FLAG-AMPKα2 was immunoprecipitated with anti-FLAG. The bound PLK1 was detected with immunoblotting by using an anti-PLK1 antibody. Nocodazole, 100 ng/mL. LC, light chain.

(C) Co-immunoprecipitation of endogenous AMPKα2 with FLAG-PLK1 in mitotic cells treated with Cdk inhibitor roscovitine. U2OS cells transiently expressing FLAG-PLK1 were synchronized in mitosis with nocodazole block, and then cells were treated with Cdk inhibitor roscovitine as well as MG132 for 1 h before collection. FLAG-PLK1 was immunoprecipitated from cell lysates with anti-FLAG antibody, and the bound AMPKα2 was analyzed by immunoblotting with anti-AMPKα2 antibody and anti-pT485 antibody. Nocodazole, 100 ng/mL. Roscovitine, 50 μM. MG132, 10 μM. HC, heavy chain.

Figure 6. *Continued*

(D) Pull-down assay of endogenous AMPKα2 in U2OS cells with recombinant GST-PBD protein. GST-PBD purified from *E. coli* was incubated with lysates of U2OS cells transiently expressing constitutively active CDK1 mutant (CDK1-AF) or kinase-dead mutant (CDK1-DN). PBD was pulled down with anti-GST, and the bound AMPKα2 was analyzed by western blotting with anti-AMPKα2 antibody and anti-pT485 antibody.

(E) Co-immunoprecipitation of FLAG-PLK1 with HA-AMPKα2 or HA-AMPKα2-485E mutant in HEK293T cells. FLAG-PLK1 was transfected with HA-AMPKα2 or HA-AMPKα2-485E mutant in HEK293T cells. FLAG-PLK1 was immunoprecipitated from cell lysates with anti-FLAG, and the precipitates were analyzed by western blotting using an anti-HA antibody. HC, heavy chain. LC, light chain.

(F) Pull-down assay of GST-PBD with MBP-AMPKα2, MBP-AMPKα2-485A, MBP-AMPKα2-485E, MBP-AMPKα1, MBP-AMPKα1-490A, or MBP-AMPKα1-490E. Purified GST-PBD protein was incubated with recombinant MBP-AMPKα2, MBP-AMPKα2-485A, MBP-AMPKα2-485E, MBP-AMPKα1, MBP-AMPKα1-490A, or MBP-AMPKα1-490E, and a pull-down assay was performed. GST-PBD was pulled down with anti-GST, and the precipitates were analyzed by using an anti-MBP antibody.

Thr485 phosphorylation promotes the binding of PLK1 to AMPKα2

Given our demonstration of the AMPKα2-PBD interaction and CDK1-primed substrate binding to the PBD of PLK1 (Elia et al., 2003b; Sillje and Nigg, 2003), we next examined whether CDK1-mediated Thr485 phosphorylation of AMPK promotes interaction between PLK1 and AMPK. U2OS cells transfected with FLAG-PBD were blocked in mitosis with nocodazole followed by anti-FLAG co-immunoprecipitation. The binding between the PBD and AMPKα2 increased in mitosis (Figure 6A). This interaction was indeed regulated by phosphorylation, because phosphatase treatment or Cdk inhibitor roscovitine treatment decreased the formation of the complexes (Figures 6B and 6C). To examine whether the CDK1 kinase activity is required for the interaction between AMPKα2 and the PBD, U2OS cells were transfected for expression of constitutive active CDK1 (T14A, Y15F) or a kinase-dead CDK1 mutant (D146N) (Iimori et al., 2016). GST pull-down assay revealed that the active CDK1, but not the kinase-dead mutant, promoted the interaction of AMPKα2 and PBD (Figure 6D). Consistent with this observation, the phosphomimic mutant T485E in AMPKα2 exhibited higher affinity with PLK1 than that of wild type (Figures 6E and S6A). We also carried out an *in vitro* pull-down assay to identify a direct interaction between PLK1 and AMPKα2 mutants. Purified truncated PBD was incubated with purified recombinant AMPKα mutants including AMPKα2-485A, AMPKα2-485E, and phospho-mimetic mutant of AMPKα1 at Thr490 (AMPKα1-490E), the site corresponding to Thr485 at AMPKα2. We found that AMPKα2-485E mutant evidently associated with PBD domain of PLK1, whereas WT AMPKα2, AMPKα2-485A, AMPKα1-490A, and AMPKα1-490E barely bound to PBD domain of PLK1 (Figure 6F), indicating the fact that priming phosphorylation still fails to enable AMPKα1 to bind to PBD domain. Thus, we conclude that priming phosphorylation of AMPKα2 at Thr485 by CDK1 promotes its interaction with PLK1, resulting in AMPKα2 activation *via* subsequent Thr172 phosphorylation by PLK1.

PLK1 specifically recognizes the STP motif in AMPKα2

Utilizing different experimental methods, our results suggest that PLK1 associates with AMPKα2 rather than AMPKα1 in mitosis (Figures 4A and 7A), which is parallel to the isoform-specific AMPKα2 activation in mitosis. However, based on the high conservation of CDK1-recognizing motif, we found that CDK1 can also phosphorylate AMPKα1 (Figure 7B) with the help of special antibody recognizing CDK substrate (Whalley et al., 2015), raising the question of how the specific binding of PLK1 to AMPKα2 and selective AMPKα2 activation are achieved in mitosis.

To identify the structural determinants underlying the isoform-specific AMPKα2-PLK1 interaction, we first compared the sequences between the AMPKα1 and AMPKα2 (Figure 7C). Although the Thr485 site is conserved among AMPKα1 and AMPKα2 subunits, the pThr(-1) position in AMPKα1 is distinctly different from that of AMPKα2, which is essential for PBD binding (Elia et al., 2003a, 2003b). Specifically, pThr(-1) position in AMPKα1 is alanine, whereas the equivalent position in AMPKα2 is serine. To evaluate our computational prediction, we constructed an AMPKα1 mutant in which the ATP motif was replaced by the STP motif. FLAG-tagged AMPKα1-STP mutant was transfected into U2OS cells, which were subsequently arrested in early mitosis by nocodazole treatment. Co-immunoprecipitation analysis indicated that immunoprecipitation of AMPKα1-STP mutant co-precipitated PLK1, whereas AMPKα1-WT did not, suggesting that AMPKα1 can interact with PLK1 upon replacement of ATP with STP motif (Figure 7D). Then, we incubated recombinant AMPKα1-STP mutant with CDK1 kinase and PLK1 kinase and measured its activity by *in vitro* kinase assay. The co-incubation with the two kinases significantly activated AMPKα1-STP mutant but failed to increase the activity of WT AMPKα1, suggesting that the increased activity of AMPKα1-STP mutant

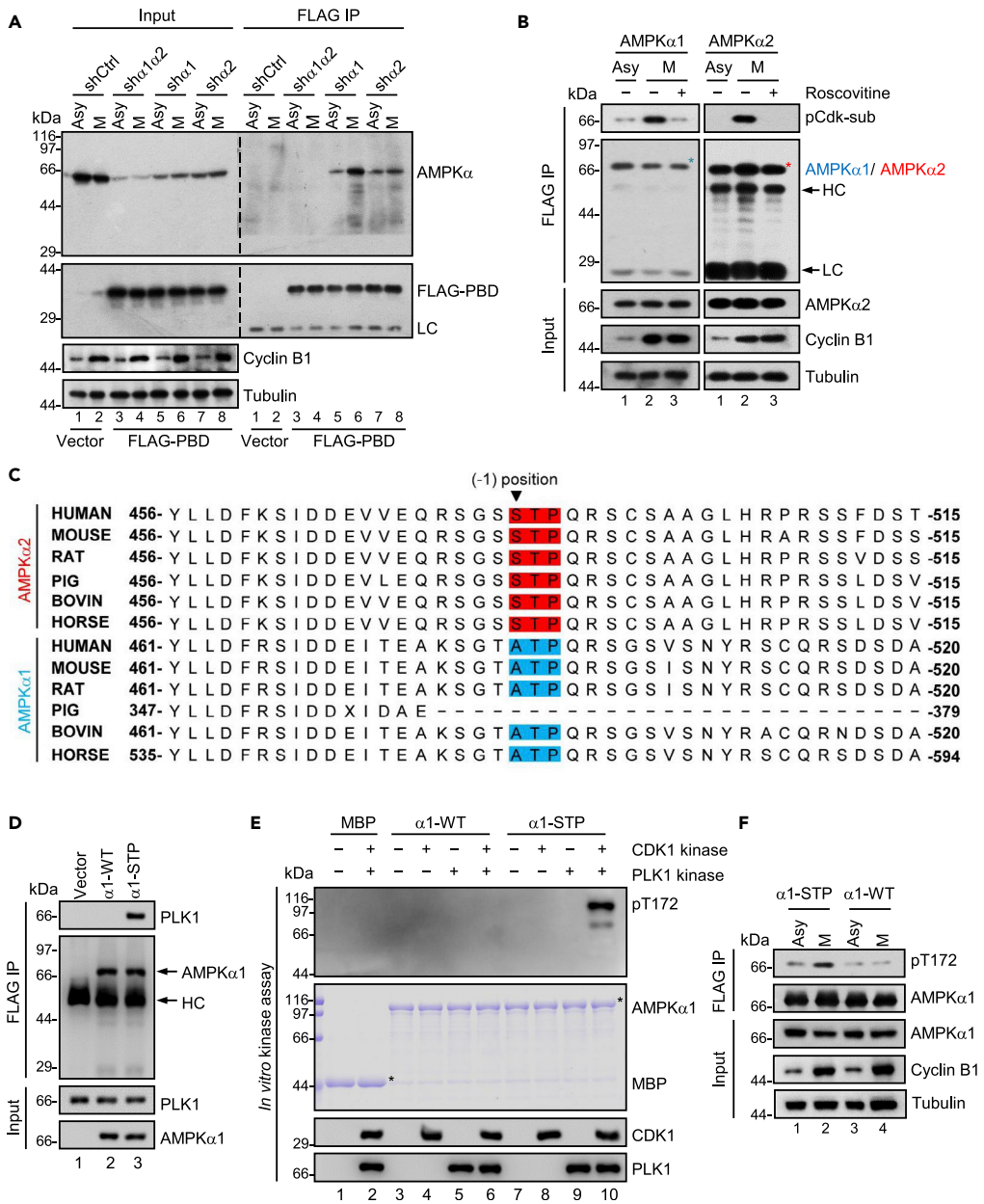

Figure 7. PLK1 specifically recognizes the STP motif in AMPKα2

(A) Co-immunoprecipitation of endogenous AMPKα with FLAG-PBD in AMPKα1-depleted or/and AMPKα2-depleted mitotic cells. U2OS cells infected with lentivirus-based particles expressing shRNA control, AMPKα1 shRNA, AMPKα2 shRNA, or AMPKα1α2 shRNA were transiently transfected with FLAG-PBD. Cells were synchronized in mitosis with nocodazole treatment. FLAG-PBD was immunoprecipitated from cell lysates with anti-FLAG, and the bound AMPKα was analyzed by western blotting with anti-AMPKα. Nocodazole, 100 ng/mL. LC, light chain.

(B) The phosphorylation levels of FLAG-AMPKα1 and FLAG-AMPKα2 immunopurified from mitotic cells treated with Cdk inhibitor roscovitine. U2OS cells stably expressing FLAG-AMPKα1 or FLAG-AMPKα2 were synchronized in mitosis with nocodazole (16 h) treatment, and then cells were treated with Cdk inhibitor roscovitine and MG132 for 1 h before collection. The exogenous AMPKα1 or AMPKα2 was immunoprecipitated from cell lysates with anti-FLAG. Phosphorylation levels of AMPKα1 and AMPKα2 were analyzed by immunoblotting with the indicated antibodies. The pCdk-sub, a specific antibody recognizing phosphorylated substrates of CDK kinase. Nocodazole, 100 ng/mL. Roscovitine, 50μM. MG132, 10 μM.

(C) Cluster alignment of the Thr485 (−1) position in AMPKα1 and AMPKα2.

Figure 7. *Continued*

(D) Co-immunoprecipitation of endogenous PLK1 with FLAG-AMPKα1 or FLAG-AMPKα1-STP mutant in mitotic cells. U2OS cells stably expressing FLAG-AMPKα1 or AMPKα1-STP mutant were synchronized in mitosis with nocodazole treatment. The exogenous AMPKα1 or AMPKα1-STP mutant was immunoprecipitated from cell lysates with anti-FLAG, and the bound PLK1 was detected by immunoblotting with the anti-PLK1 antibody. Nocodazole, 100 ng/mL.

(E) *In vitro* kinase assays using recombinant MBP-tagged AMPKα1 or AMPKα1-STP mutant, in the presence of CDK1-Cyclin B1 kinase, or PLK1 kinase, or with CDK1-Cyclin B1 added to the kinase assay first followed by PLK1 addition. Samples were subjected to immunoblotting with the indicated antibodies and CBB staining.

(F) The phosphorylation level of Thr172 of AMPKα1 or AMPKα1-STP mutant immunopurified from mitotic cells. U2OS cells stably expressing FLAG-AMPKα1 or FLAG-AMPKα1-STP mutant were synchronized in mitosis with nocodazole block. The exogenous AMPKα1 or AMPKα1-STP mutant was immunoprecipitated with anti-FLAG and was analyzed by western blotting for pT172 level. Nocodazole, 100 ng/mL.

comes from the alanine-to-serine replacement (Figure 7E). We also purified wild-type FLAG-AMPKα1 and the A489S mutant AMPKα1 from mitotic cells and tested the activity of AMPKα1. As shown in Figures 7F and S7A, AMPKα1 A489S mutant with the same centrosomal localization (Figure S7B) exhibited higher phosphorylation level at Thr172 compared with the AMPKα1 WT, whereas the wild type remains unchanged, suggesting a critical role of serine at the pThr(-1) position in the specificity of the STP motif for PLK1-dependent phosphorylation of AMPKα2. Thus, we reason that the (−1) position at the STP motif of AMPKα2 (Ser484 site) is the key position for isoform-specific AMPKα2 activation, and engineering the corresponding site at AMPKα1 enables its activation in mitosis.

AMPKα1-STP mutant rescues the mitotic phenotypes in AMPKα2-deficient cells

To further test the function of CDK1-mediated AMPK activation in mitosis, we re-introduced the AMPKα2 wild type or the T485A mutant in AMPKα2-deficient cells, respectively. Quantitative analyses of more than 100 cells in each group show that expression of AMPKα2-T485A was unable to rescue the chromosome alignment errors and anaphase defects seen in AMPKα2-deficient cells (Figures 8A–8C), revealing a temporal coordination of the CDK1/PLK1-AMPKα2 signaling axis in the metaphase-anaphase transition to ensure maintenance of the genomic stability.

If AMPKα2 is specifically required for accurate mitosis, expression of AMPKα1-A489S mutant that restores the STP motif and can serve as a PLK1 substrate might rescue the mitotic phenotypes seen in AMPKα2-deficient cells. To test this possibility, we introduced FLAG-AMPKα1 wild type or the A489S mutant in AMPKα2 shRNA-treated cells and scored chromosome alignment at metaphase and anaphase chromatid separation. Consistent with our prediction, quantitative analyses of 100 transfected cells in each category showed that AMPKα1-A489S, but not wild-type AMPKα1, could rescue the chromosome alignment errors and anaphase defects seen in AMPKα2-deficient cells (Figures 8D–8F). Thus, we conclude that CDK1-elicited priming phosphorylation of AMPKα2 promotes activation of AMPKα2 by PLK1 and orchestrates faithful mitotic progression (Figure 8G).

DISCUSSION

Several lines of evidence suggest a role of AMPK during mitosis (Li et al., 2018; Mao et al., 2013; Thaiparambil et al., 2012). Our findings here uncovered a mechanism of action underlying isoform-specific regulation that integrates sequential phosphorylation by CDK1 and PLK1 to AMPKα2 activation and function in orchestrating genomic stability in mitosis. Our study identified that PLK1-dependent phosphorylation of AMPKα2 drives mitosis, independent of LKB1 or CAMKKβ. This mitosis-elicited phosphorylation of AMPKα2 is a novel non-canonical activation of Thr172, which depends on CDK1-primed Thr485 phosphorylation. Thus, Thr485 of AMPKα is a *bona fide* substrate of CDK1-Cyclin B1. Importantly, PLK1-mediated phosphorylation is specific to AMPKα2 due to the PBD domain of PLK1 specifically recognizing the "STP" motif in AMPKα2 but not the equivalent "ATP" motif in AMPKα1. Significantly, expression of AMPKα1 containing an engineered STP motif rescued the mitotic phenotype seen in AMPKα2-depleted cells.

An elegant crystallography study revealed the atomic structures of the mammalian AMPK heterotrimeric complex and their structure-activity relationship (Xiao et al., 2011). However, the AMPK complex was engineered by removing the flexible S-T stretch containing Thr485. Interestingly, our study suggests that this flexible region functions as a phosphorylation-sensitive switch that regulates the specificity of AMPKα2 kinase in mitosis. The negative charge of the ST-stretch via CDK1-elicited phosphorylation enables interaction with the PBD domain of PLK1 and the ensuing phosphorylation of Thr172 by PLK1. These data provide

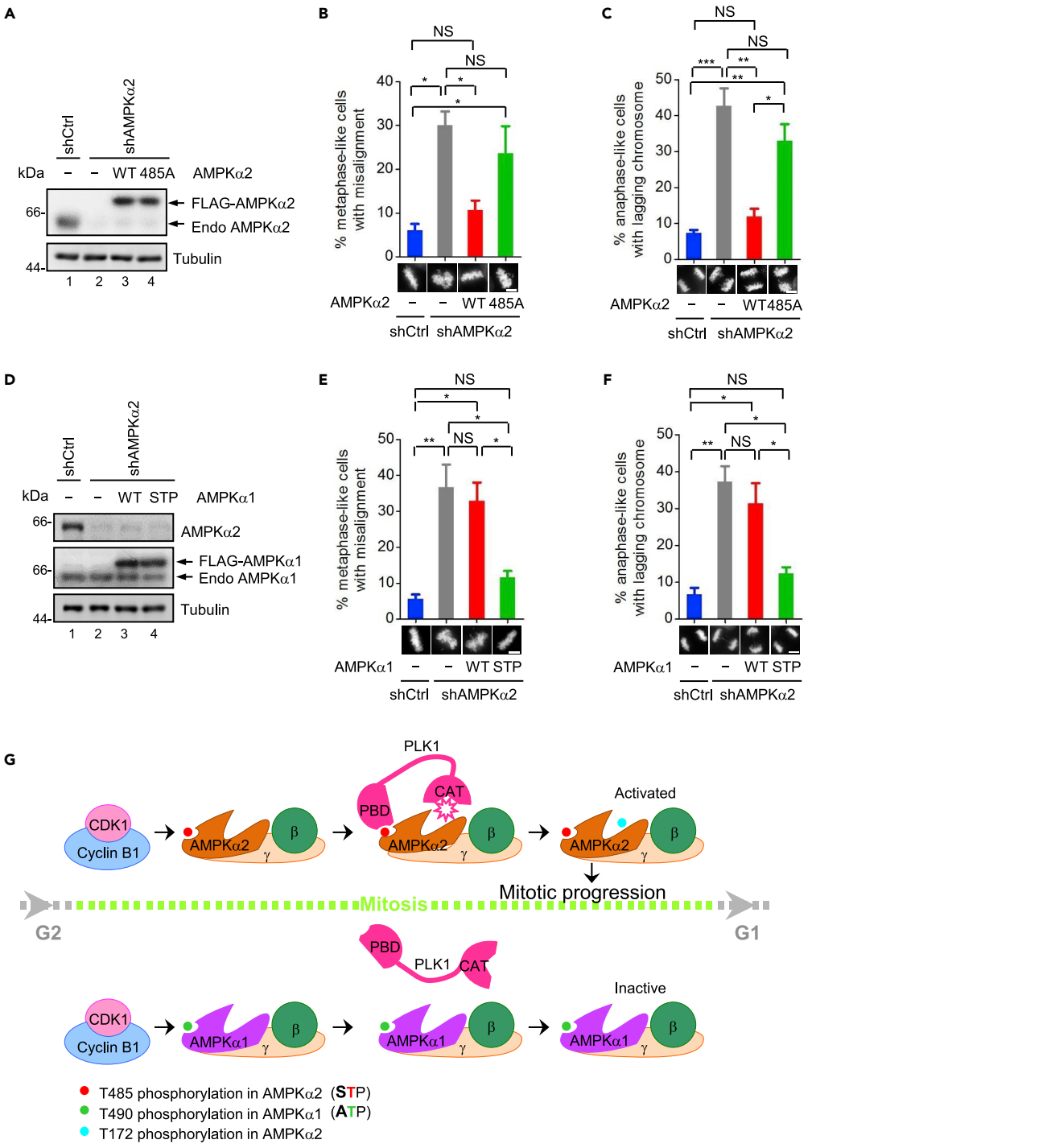

Figure 8. AMPKα1-STP mutant rescues the mitotic phenotypes in AMPKα2-deficient cells

(A) Protein levels of AMPKα2 in AMPKα2-depleted HeLa cells expressing WT AMPKα2 or AMPKα2-485A mutant. Endo AMPKα2, endogenous AMPKα2.

(B and C) HeLa cells stably expressing AMPKα2 shRNA were transfected with FLAG-tagged AMPKα2 or AMPKα2-485A mutant. After fixation, cells were stained with DAPI, and the phenotypes were determined under a DeltaVision microscope. Representative phenotypes of each group are shown at the bottom (n = 120 for each group). Data represent mean ± SEM. All data passed the Shapiro-Wilk normality test. Ordinary one-way ANOVA followed by Tukey's post hoc test was used to determine statistical significance. NS (not significant) indicates $p > 0.05$. (B) *p = 0.0081; *p = 0.0261; *p = 0.0405. (C) ***p = 0.0005; **p = 0.0013; **p = 0.0041; *p = 0.0132. Scale bars, 10 μm. The average +/− SEM of each panel in

Figure 8. *Continued*

(B) was 6.000 ± 1.528 (%), 30.00 ± 3.215 (%), 10.67 ± 2.186 (%), and 23.67 ± 6.173 (%). The average +/− SEM of each panel in (C) was 7.333 ± 0.8819 (%), 42.67 ± 4.910 (%), 12.00 ± 2.082 (%), and 33.00 ± 4.619 (%).

(D) Protein levels of AMPKα1 and AMPKα2 in AMPKα2-depleted HeLa cells overexpressing WT AMPKα1 or AMPKα1-STP mutant. Endo AMPKα1, endogenous AMPKα1.

(E and F) HeLa cells stably expressing AMPKα2 shRNA were transfected with FLAG-tagged AMPKα1 or AMPKα1-STP mutant. After fixation, cells were stained with DAPI and the phenotypes were determined under a DeltaVision microscope. Representative phenotypes of each group are shown at the bottom (n = 120 for each group). Data represent mean ± SEM. All data passed the Shapiro-Wilk normality test. Ordinary one-way ANOVA followed by Tukey's post hoc test was used to determine statistical significance. NS (not significant) indicates $p > 0.05$. (E) $^{**}p = 0.0035$; $^{*}p = 0.0074$; $^{*}p = 0.0123$; $^{*}p = 0.0285$. (F) $^{**}p = 0.0017$; $^{*}p = 0.0061$; $^{*}p = 0.0066$; $^{*}p = 0.0275$. Scale bars, 10 μm. The average +/− SEM of each panel in (E) was 5.667 ± 1.202 (%), 36.67 ± 6.333 (%), 33.00 ± 5.033 (%), and 11.67 ± 1.764 (%). The average +/− SEM of each panel in (F) was 6.667 ± 1.856 (%), 37.33 ± 4.177 (%), 31.33 ± 5.548 (%), and 12.33 ± 1.764 (%).

(G) Schematic model for PLK1-mediated AMPKα2 activation in mitosis. During mitosis, AMPK is first phosphorylated by the priming kinase CDK1, and this provides a docking site for direct involvement of PLK1 in AMPKα2 activation through directly phosphorylating AMPKα2 at the active site. Once the sequential phosphorylated molecules are activated, they participate in ensuring mitotic progression. However, the variation of PLK1 docking site, that is STP located in AMPKα2 whereas ATP in AMPKα1, results in the specific binding of PLK1 to AMPKα2 and then the specific AMPKα2 activation, even though AMPKα1 can also be phosphorylated by CDK1.

mechanistic insight on the CDK1 and PLK1 sequential phosphorylation and activation of AMPKα2 in mitosis. During the preparation of this manuscript, Stuffer and colleagues identified the phosphorylation of Ser377 and Thr485 of AMPKα2 in mitosis (Stauffer et al., 2019), which is consistent with our mass spectrometric identification of Ser345, Ser377, and Thr485. The aforementioned study was primarily focused on phosphorylation of Ser377, which was shown to be independent of Thr485 phosphorylation in the same study, and its contribution to mitosis. Thus, future work should delineate the respective roles of phosphorylation of Ser377 and Thr485 in AMPKα2 signaling in mitosis. It would be great interest to illuminate the temporal dynamics of Ser377 and Thr485 phosphorylation in mitosis and their relative contribution to enzymatic activities in mitosis.

AMPK shows strong centrosomal localization during mitosis (Figure S1A), which is consistent with previous reports. Meanwhile, we also find the kinetochore localization of pT172-AMPK in Figure 1B, and this centromeric signal can also be suppressed by PLK1 depletion (Figure 3C). However, we did not find significant kinetochore localization of AMPK itself (Figure 4B). Even though there is slight kinetochore localization of AMPK in metaphase cells in Figure S1B, we failed to detect the same localization at other stages. Therefore, it is worthy to further study the AMPK's kinetochore localization and its function in mitosis.

Although our results confirm the role of AMPKα2 in orchestrating genomic stability in mitosis, we also note the fact that AMPKα2 KO mice can still survive without major defects. This spice-and-context distinct phenotype has led us to speculate on the functional specificity of AMPKα2 in mouse and human cell lines. Future studies will be centered on the specific function of AMPKα2 in vertebrates.

Our results provide mechanistic insight into how priming phosphorylation at Thr485 by CDK1-Cyclin B1 enables AMPK to interact with the polo-box domain of PLK1. Interestingly, our results also showed that PLK1-mediated AMPK activation in mitosis was selective to AMPKα2 but not AMPKα1. Depletion of AMPKα2 prevented activation of AMPK in mitosis. The underlying mechanism we uncovered indicates that selective AMPKα2 activation in mitosis is due to the PBD domain of PLK1 being able to only recognize the S-pT-P motif in AMPKα2, but not the A-pT-P motif in AMPKα1, thus providing a molecular basis for isoform-specific AMPKα2 activity in mitosis.

This and previous studies indicate that AMPK has important roles in the regulation of cell division. In fact, selective regulation for AMPKα1 and AMPKα2 was reported previously as a result of AKT phosphorylation of the α1 subunit but not AMPKα2 (Hawley et al., 2014). We are still at the early stages of understanding the detailed mechanisms underlying isoform-specific AMPKα2-dependent regulation of chromosome segregation, spindle orientation, and spindle checkpoint. Further studies will be needed to fully understand and tease out the physiological significance of isoform-specific signaling cascades involving AMPK in mitosis. The discovery of sequential phosphorylation of AMPKα2 by CDK1-Cyclin B1 and PLK1 and its

specific requirement in mitosis contributes to a deeper understanding of the isoform-specific AMPK signaling in mitosis and may represent a unique readout for chemical biological intervention targeting AMPKα2.

Limitations of the study

This study reveals AMPKα2 is activated by sequential phosphorylation by CDK1 and PLK1 in mitosis. Mitotic AMPKα2 activation is essential for proper chromosomal segregation. However, we still lack the direct substrates of AMPK in spindle pole, which regulates mitosis progression.

We observed evident pT172-AMPK signal in kinetochore, but we cannot confirm AMPK's kinetochore localization with GFP-AMPK stable cell line. Is AMPK targeted to kinetochore in some special conditions? This may be resolved in the future study.

Resource availability

Lead contact

Further information and requests for resources should be directed to and will be fulfilled by the lead contact, Xuebiao Yao (yaoxb@ustc.edu.cn).

Materials availability

Materials and the information used for the experiments are available upon reasonable request.

Data and code availability

Further information about data supporting the conclusions of this manuscript will be made available by the lead contact to any qualified researcher.

METHODS

All methods can be found in the accompanying transparent methods supplemental file.

SUPPLEMENTAL INFORMATION

Supplemental information can be found online at https://doi.org/10.1016/j.isci.2021.102363.

ACKNOWLEDGMENTS

We are grateful to Prof. Jiawei Wu for support. We thank all the members of our laboratories for discussion and Dr. O. Rom for assistance with statistical analysis. This work was supported in part by the National Key Research and Development Program of China (2017YFA0503600, 2016YFA0100500); National Natural Science Foundation of China (31621002, 32090040, 91854203, 91853115, 21922706, 31871359, 31970655, and 31671405); "Strategic Priority Research Program" of the Chinese Academy of Sciences (XDB19000000); the Fundamental Research Funds for the Central Universities (WK2070000194, KB2070000023, YD2070006001); MOE Innovative team (IRT_17R102).

AUTHORS CONTRIBUTION

X.Y. conceived the project. J.L. and Y.H. designed and performed most experiments. X.L., M.W., and L.X. designed and performed cell biological experiments. L.Z. and J.Z. performed mass spectrometry analyses. MTGB performed statistical analyses and data interpretation. All authors contributed to the writing or editing of the manuscript.

DECLARATION OF INTERESTS

The authors declare no competing financial interests.

Received: September 10, 2020
Revised: February 15, 2021
Accepted: March 23, 2021
Published: April 23, 2021

REFERENCES

Banko, M.R., Allen, J.J., Schaffer, B.E., Wilker, E.W., Tsou, P., White, J.L., Villen, J., Wang, B., Kim, S.R., Sakamoto, K., et al. (2011). Chemical genetic screen for AMPKalpha2 substrates uncovers a network of proteins involved in mitosis. Mol. Cell *44*, 878–892.

Dasgupta, B., and Chhipa, R.R. (2016). Evolving lessons on the complex role of AMPK in normal physiology and cancer. Trends Pharmacol. Sci. *37*, 192–206.

Elia, Andrew E.H., Cantley, L.C., and Yaffe, Michael B. (2003a). Proteomic screen finds pSer/pThr–binding domain localizing Plk1 to mitotic Substrates. Science *299*, 1228–1231.

Elia, Andrew E.H., Rellos, P., Haire, Lesley F., Chao, Jerry W., Ivins, Frank J., Hoepker, Katja, Mohammad, Duaa, Cantley, Lewis C., Smerdon, Stephen J., and Yaffe, Michael B. (2003b). The molecular basis for phosphodependent substrate targeting and regulation of plks by the polo-box domain. Cell *115*, 83–95.

Garcia-Alvarez, B., de Carcer, G., Ibanez, S., Bragado-Nilsson, E., and Montoya, G. (2007). Molecular and structural basis of polo-like kinase 1 substrate recognition: implications in centrosomal localization. Proc. Natl. Acad. Sci. U S A *104*, 3107–3112.

Godek, K.M., Kabeche, L., and Compton, D.A. (2015). Regulation of kinetochore-microtubule attachments through homeostatic control during mitosis. Nat. Rev. Mol. Cell Biol. *16*, 57–64.

Golsteyn, R.M., Mundt, K.E., Fry, A.M., and Nigg, E.A. (1995). Cell cycle regulation of the activity and subcellular localization of Plk1, a human protein kinase implicated in mitotic spindle function. J. Cell Biol. *129*, 1617–1628.

Hawley, S.A., Pan, D.A., Mustard, K.J., Ross, L., Bain, J., Edelman, A.M., Frenguelli, B.G., and Hardie, D.G. (2005). Calmodulin-dependent protein kinase kinase-beta is an alternative upstream kinase for AMP-activated protein kinase. Cell Metab. *2*, 9–19.

Hawley, S.A., Ross, F.A., Gowans, G.J., Tibarewal, P., Leslie, N.R., and Hardie, D.G. (2014). Phosphorylation by Akt within the ST loop of AMPK-alpha1 down-regulates its activation in tumour cells. Biochem. J. *459*, 275–287.

Hutterer, A., Berdnik, D., Wirtz-Peitz, F., Zigman, M., Schleiffer, A., and Knoblich, J.A. (2006). Mitotic activation of the kinase Aurora-A requires its binding partner Bora. Dev. Cell *11*, 147–157.

Iimori, M., Watanabe, S., Kiyonari, S., Matsuoka, K., Sakasai, R., Saeki, H., Oki, E., Kitao, H., and Maehara, Y. (2016). Phosphorylation of EB2 by Aurora B and CDK1 ensures mitotic progression and genome stability. Nat. Commun. *7*, 11117.

Jackman, M., Lindon, C., Nigg, E.A., and Pines, J. (2003). Active cyclin B1-Cdk1 first appears on centrosomes in prophase. Nat. Cell Biol. *5*, 143–148.

Joukov, V., and De Nicolo, A. (2018). Aurora-PLK1 cascades as key signaling modules in the regulation of mitosis. Sci. Signal. *11*, eaar4195.

Kishimoto, A., Ogura, T., and Esumi, H. (2006). A pull-down assay for 5′ AMP-activated protein kinase activity using the GST-fused protein. Mol. Biotechnol. *32*, 17–21.

Lee, I.J., Lee, C.W., and Lee, J.H. (2015). CaMKKbeta-AMPKalpha2 signaling contributes to mitotic Golgi fragmentation and the G2/M transition in mammalian cells. Cell Cycle *14*, 598–611.

Lee, H., Zandkarimi, F., Zhang, Y., Meena, J.K., Kim, J., Zhuang, L., Tyagi, S., Ma, L., Westbrook, T.F., Steinberg, G.R., et al. (2020). Energy-stress-mediated AMPK activation inhibits ferroptosis. Nat. Cell Biol. *22*, 225–234.

Li, Q.R., Yan, X.M., Guo, L., Li, J., and Zang, Y. (2018). AMPK regulates anaphase central spindle length by phosphorylation of KIF4A. J. Mol. Cell Biol. *10*, 2–17.

Lin, S.C., and Hardie, D.G. (2018). AMPK: sensing glucose as well as cellular energy status. Cell Metab. *27*, 299–313.

Lopez-Mejia, I.C., Lagarrigue, S., Giralt, A., Martinez-Carreres, L., Zanou, N., Denechaud, P.D., Castillo-Armengol, J., Chavey, C., Orpinell, M., Delacuisine, B., et al. (2017). CDK4 Phosphorylates AMPKalpha2 to inhibit its activity and repress fatty acid oxidation. Mol. Cell *68*, 336–349.

Macurek, L., Lindqvist, A., Lim, D., Lampson, M.A., Klompmaker, R., Freire, R., Clouin, C., Taylor, S.S., Yaffe, M.B., and Medema, R.H. (2008). Polo-like kinase-1 is activated by aurora A to promote checkpoint recovery. Nature *455*, 119–123.

Mao, L., Li, N., Guo, Y., Xu, X., Gao, L., Xu, Y., Zhou, L., and Liu, W. (2013). AMPK phosphorylates GBF1 for mitotic Golgi disassembly. J. Cell Sci. *126*, 1498–1505.

Miyamoto, T., Oshiro, N., Yoshino, K., Nakashima, A., Eguchi, S., Takahashi, M., Ono, Y., Kikkawa, U., and Yonezawa, K. (2008). AMP-activated protein kinase phosphorylates Golgi-specific brefeldin A resistance factor 1 at Thr1337 to induce disassembly of Golgi apparatus. J. Biol. Chem. *283*, 4430–4438.

Schaar, B.T., Chan, G.K., Maddox, P., Salmon, E.D., and Yen, T.J. (1997). CENP-E function at kinetochores is essential for chromosome alignment. J. Cell biol. *139*, 1373–1382.

Seki, A., Coppinger, J.A., Jang, C.Y., Yates, J.R., and Fang, G. (2008). Bora and the kinase Aurora a cooperatively activate the kinase Plk1 and control mitotic entry. Science *320*, 1655–1658.

Shaw, R.J., Kosmatka, M., Bardeesy, N., Hurley, R.L., Witters, L.A., DePinho, R.A., and Cantley, L.C. (2004). The tumor suppressor LKB1 kinase directly activates AMP-activated kinase and regulates apoptosis in response to energy stress. Proc. Natl. Acad. Sci. U S A *101*, 3329–3335.

Sillje, H.H., and Nigg, E.A. (2003). Signal transduction. Capturing polo kinase. Science *299*, 1190–1191.

Stauffer, S., Zeng, Y., Santos, M., Zhou, J., Chen, Y., and Dong, J. (2019). Cyclin-dependent kinase 1-mediated AMPK phosphorylation regulates chromosome alignment and mitotic progression. J. Cell Sci. *132*, jcs236000.

Steegmaier, M., Hoffmann, M., Baum, A., Lenart, P., Petronczki, M., Krssak, M., Gurtler, U., Garin-Chesa, P., Lieb, S., Quant, J., et al. (2007). BI2536, a potent and selective inhibitor of polo-like kinase 1, inhibits tumor growth in vivo. Curr. Biol. *17*, 316–322.

Sullivan, J.E., Carey, F., Carling, D., and Beri, R.K. (1994). Characterisation of 5′-AMP-activated protein kinase in human liver using specific peptide substrates and the effects of 5′-AMP analogues on enzyme activity. Biochem. Biophys. Res. Commun. *200*, 1551–1556.

Thaiparambil, J.T., Eggers, C.M., and Marcus, A.I. (2012). AMPK regulates mitotic spindle orientation through phosphorylation of myosin regulatory light chain. Mol. Cell Biol. *32*, 3203–3217.

Tripodi, F., Fraschini, R., Zocchi, M., Reghellin, V., and Coccetti, P. (2018). Snf1/AMPK is involved in the mitotic spindle alignment in Saccharomyces cerevisiae. Sci. Rep. *8*, 5853.

Vazquez-Martin, A., Oliveras-Ferraros, C., and Menendez, J.A. (2009). The active form of the metabolic sensor: AMP-activated protein kinase (AMPK) directly binds the mitotic apparatus and travels from centrosomes to the spindle midzone during mitosis and cytokinesis. Cell Cycle *8*, 2385–2398.

Vazquez-Martin, A., Oliveras-Ferraros, C., Cufi, S., and Menendez, J.A. (2011). Polo-like kinase 1 regulates activation of AMP-activated protein kinase (AMPK) at the mitotic apparatus. Cell Cycle *10*, 1295–1302.

Vazquez-Martin, A., Cufi, S., Oliveras-Ferraros, C., and Menendez, J.A. (2012). Polo-like kinase 1 directs the AMPK-mediated activation of myosin regulatory light chain at the cytokinetic cleavage furrow independently of energy balance. Cell Cycle *11*, 2422–2426.

Wan, L., Xu, K., Wei, Y., Zhang, J., Han, T., Fry, C., Zhang, Z., Wang, Y.V., Huang, L., Yuan, M., et al. (2018). Phosphorylation of EZH2 by AMPK suppresses PRC2 methyltransferase activity and oncogenic function. Mol. Cell *69*, 279–291.

Whalley, H.J., Porter, A.P., Diamantopoulou, Z., White, G.R., Castaneda-Saucedo, E., and Malliri, A. (2015). Cdk1 phosphorylates the Rac activator Tiam1 to activate centrosomal Pak and promote mitotic spindle formation. Nat. Commun. *6*, 7437.

Woods, A., Johnstone, S.R., Dickerson, K., Leiper, F.C., Fryer, L.G., Neumann, D., Schlattner, U., Wallimann, T., Carlson, M., and Carling, D. (2003). LKB1 is the upstream kinase in the AMP-activated protein kinase cascade. Curr. Biol. *13*, 2004–2008.

Xiao, B., Sanders, M.J., Underwood, E., Heath, R., Mayer, F.V., Carmena, D., Jing, C., Walker, P.A., Eccleston, J.F., Haire, L.F., et al. (2011). Structure of mammalian AMPK and its regulation by ADP. Nature *472*, 230–233.

Yang, Q., Xu, J., Ma, Q., Liu, Z., Sudhahar, V., Cao, Y., Wang, L., Zeng, X., Zhou, Y., Zhang, M., et al. (2018). PRKAA1/AMPKalpha1-driven glycolysis in endothelial cells exposed to disturbed flow protects against atherosclerosis. Nat. Commun. *9*, 4667.

Zhao, H., Li, T., Wang, K., Zhao, F., Chen, J., Xu, G., Zhao, J., Li, T., Chen, L., Li, L., et al. (2019). AMPK-mediated activation of MCU stimulates mitochondrial Ca(2+) entry to promote mitotic progression. Nat. Cell Biol. *21*, 476–486.

iScience, Volume *24*

Supplemental information

AMPKα2 activation by an energy-independent signal ensures chromosomal stability during mitosis

Jianlin Lu, Yuanyuan Huang, Li Zhan, Ming Wang, Leilei Xu, McKay Mullen, Jianye Zang, Guowei Fang, Zhen Dou, Xing Liu, Wei Liu, Minerva Garcia-Barrio, and Xuebiao Yao

Supplemental Figures

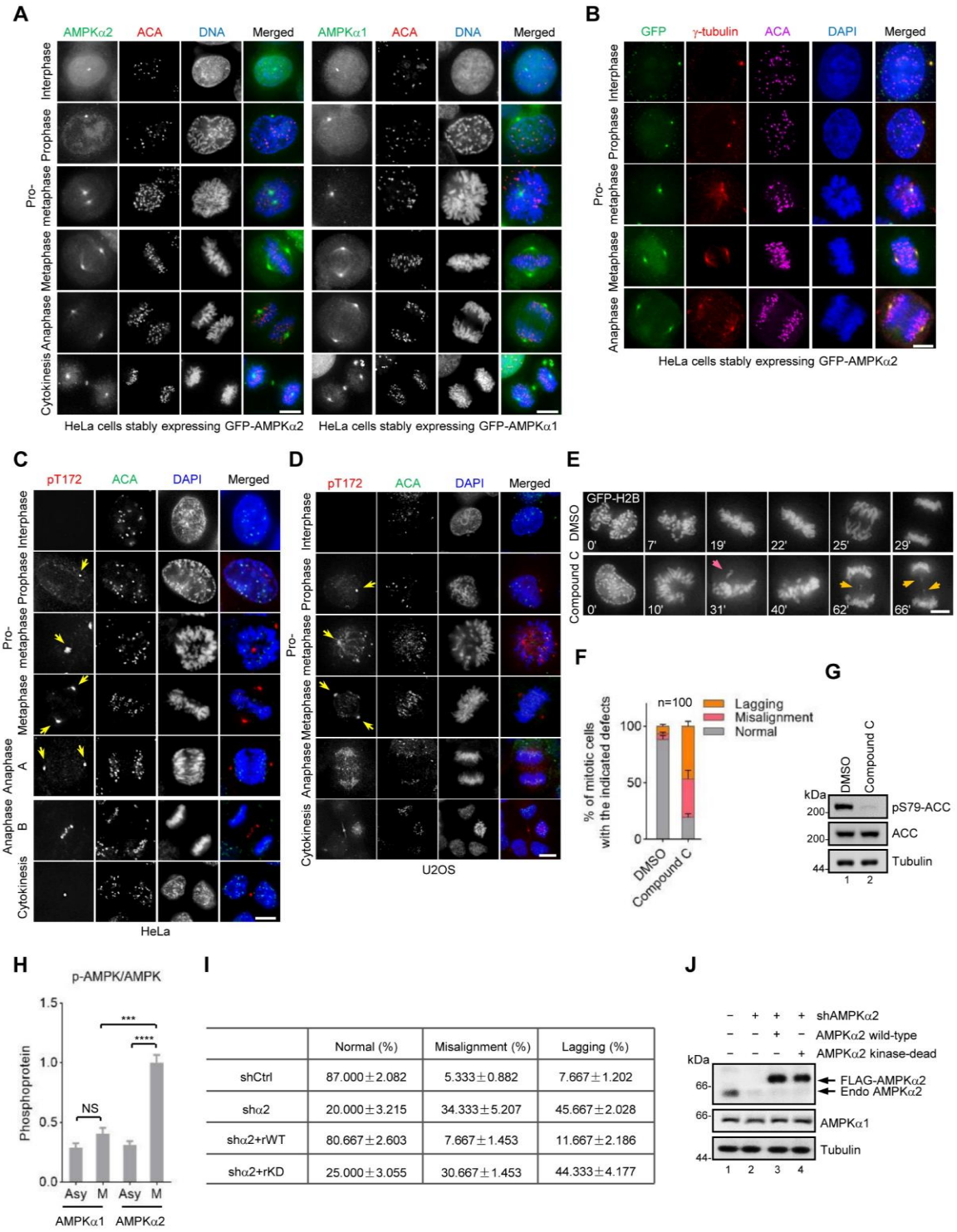

	Normal (%)	Misalignment (%)	Lagging (%)
shCtrl	87.000±2.082	5.333±0.882	7.667±1.202
shα2	20.000±3.215	34.333±5.207	45.667±2.028
shα2+rWT	80.667±2.603	7.667±1.453	11.667±2.186
shα2+rKD	25.000±3.055	30.667±1.453	44.333±4.177

Figure S1. AMPKα2 activation is essential for faithful chromosomal separation (related to Figure 1)

A, Both AMPKα1 and AMPKα2 are located on centrosomes during different mitotic stages. HeLa

cells stably expressing GFP-AMPKα1 and GFP-AMPKα2 were treated with double thymidine block (2.5 mM thymidine, 16 h each time) followed by releasing for 8 h. Cells were fixed, permeabilized, and stained for ACA (red) and DAPI (blue). Scale bars, 10 μm. **B**, Subcellular localization of AMPKα2 in different mitotic stages. HeLa cells stably expressing GFP-AMPKα2 were treated with double thymidine block (2.5 mM thymidine, 16 h each time) followed by releasing for 8 h. Cells were fixed, permeabilized, and stained for γ-tubulin (red), ACA (magenta), and DAPI (blue). Scale bar, 10 μm. **C**-**D**, Subcellular localization of active form AMPK in different mitotic stages. HeLa cells (C) and U2OS cells (D) were treated with double thymidine block (2.5 mM thymidine, 16 h each time) followed by releasing for 8 h. Cells were fixed, permeabilized, and stained for endogenous phospho-AMPK (red), ACA (green), and DAPI (blue). ACA, anti-centromere autoimmune serum, the marker of kinetochores. Scale bar, 10 μm. **E**, HeLa cells stably expressing GFP-H2B were treated with 10 μM Compound C after mitotic entry. Representative phenotypes were visualized with GFP-H2B by time-lapse microscopy. The pink arrows indicate misaligned chromosomes, and the orange arrows indicate lagging chromosomes. Numbers at the bottom left of images indicate elapsed time in minutes. Scale bar, 10 μm. **F**, Phenotypic statistics of (E). Data represent mean ± SEM. The experiment was repeated three times independently (n=100). The average +/- SEM of each panel in DMSO group was 88.667 ± 2.028 (Normal, %), 4.667 ± 0.882 (Misalignment, %), 6.667 ± 1.202 (Lagging, %); the average +/- SEM of each panel in Compound C group was 19.667 ± 1.764 (Normal, %), 34.000 ± 4.359 (Misalignment, %), 46.333 ± 2.603 (Lagging, %). **G**, HeLa cells were treated with Compound C (10 μM) for 2 h, and cell lysates were analyzed by Western blotting using the indicated antibodies. The pS79-ACC was used as a marker for AMPK activity. **H**, Quantification of pT172 levels as in Figure 1E. Data represent mean ± SEM. The experiment was repeated three times independently. Ordinary one-way ANOVA followed by Tukey's multiple comparisons test was used to determine statistical significance. NS (not significant) indicates $p>0.05$. ***$p=0.0001$. ****$p<0.0001$. The average +/- SEM of each panel was 0.2881 ± 0.03766, 0.4051 ± 0.04898, 0.3126 ± 0.03037, 1.000 ± 0.06616. **I**, The average +/- SEM of each panel as in Figure 1G. **J**, Protein levels of AMPKα2 in AMPKα2-depleted cells that expressing WT AMPKα2 or kinase-dead mutant. HeLa cells stably expressing AMPKα2 shRNA were infected with lentivirus-based particles expressing wild-type AMPKα2 or the kinase-dead mutant (AMPKα2 T172A). Cell lysates were analyzed by Western blotting using the AMPKα2 antibody.

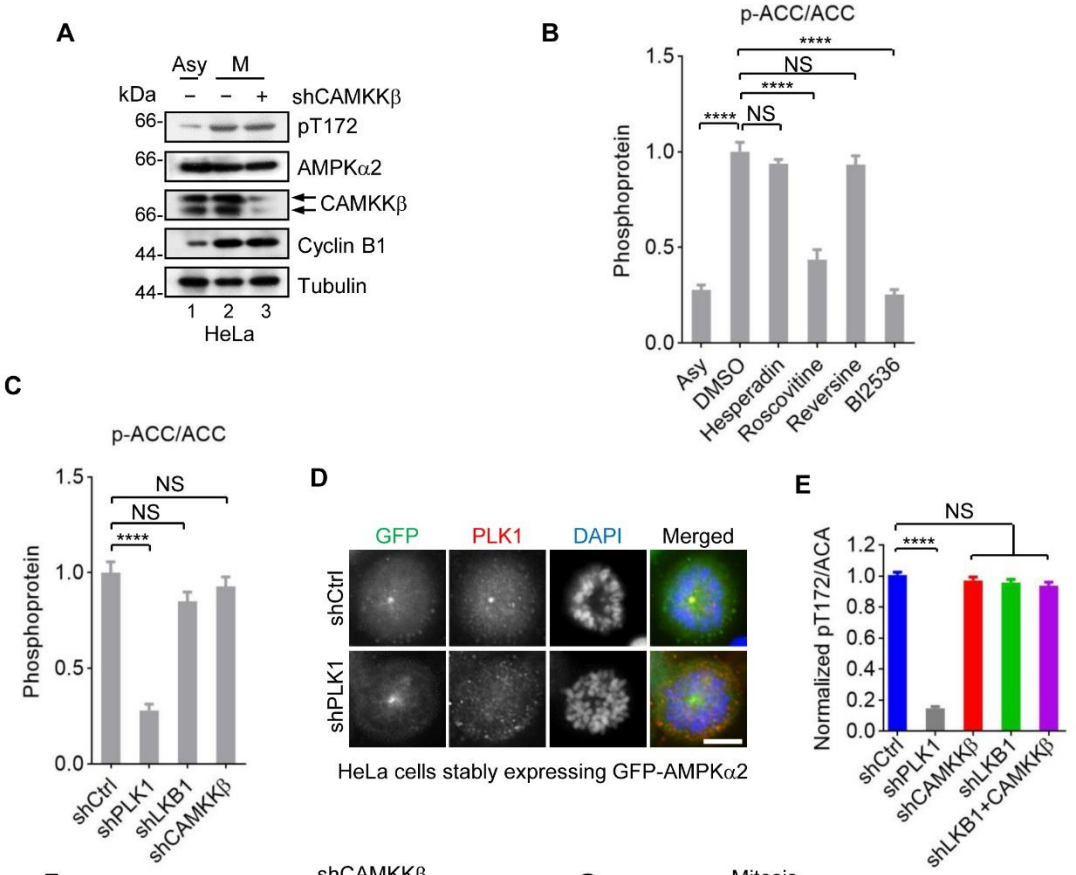

H

	shCtrl	shPLK1	shCAMKKβ	dKD
Untreated	1.000±0.115	0.094±0.016	0.919±0.138	0.059±0.004
Starvation	1.003±0.138	0.591±0.101	0.685±0.059	0.067±0.009

Figure S2. PLK1-dependent mitotic AMPKα2 activation is not regulated by energy stress (related to Figure 2)

A, Activity of AMPKα2 in CAMKKβ-depleted HeLa cells. HeLa cells stably expressing CAMKKβ shRNA were arrested in mitosis by treatment with 100 ng/ml nocodazole for 16 h. Whole-cell lysates (WCL) were separated by SDS-PAGE and immunoblotted with anti-pT172-AMPK to examine

AMPKα2 kinase activity. Asy, asynchronous. M, mitotic. **B**, Quantification of pS79-ACC levels as in Figure 2B. Data represent mean ± SEM. The experiment was repeated three times independently. Ordinary one-way ANOVA followed by Tukey's multiple comparisons test was used to determine statistical significance. NS (not significant) indicates p>0.05. ****p<0.0001. The average +/- SEM of each panel was 0.2793 ± 0.02508, 1.000 ± 0.05051, 0.9382 ± 0.02229, 0.4366 ± 0.05251, 0.9342 ± 0.04557, 0.2553 ± 0.02422. **C**, Quantification of pS79-ACC levels as in Figure 2C. Data represent mean ± SEM. The experiment was repeated three times independently. Ordinary one-way ANOVA followed by Tukey's multiple comparisons test was used to determine statistical significance. NS (not significant) indicates p>0.05. ****p<0.0001. The average +/- SEM of each panel was 1.000 ± 0.05703, 0.2807 ± 0.03235, 0.8515 ± 0.04756, 0.9291 ± 0.04939. **D**, Subcellular localization of AMPKα2 in PLK1-depleted HeLa cells. HeLa cells stably expressing GFP-AMPKα2 were infected with lentivirus-based particles expressing PLK1 shRNA and then were treated with double thymidine block (2.5 mM thymidine, 16 h each time) followed by releasing for 8 h. Cells were fixed and stained with the PLK1 antibody. Scale bar, 10 μm. **E**, Quantification of immunofluorescence intensity as in Figure 2D. Data represent mean ± SEM. The experiment was repeated three times independently (n=60). The Non-parametric Kruskal-Wallis test followed by Dunn's multiple comparisons test was used for the analysis. ****p<0.0001. NS (not significant) indicates p>0.05 compared to control. The average +/- SEM of each panel was 1.006 ± 0.01828, 0.1474 ± 0.01147, 0.9725 ± 0.02046, 0.9577 ± 0.02079, 0.9376 ± 0.02239. **F**, Knockdown efficiency of PLK1 shRNA, LKB1 shRNA (shLKB1-#1 and shLKB1-#2), and CAMKKβ shRNA. U2OS cells stably expressing indicated shRNAs were analyzed by Western blotting to identify knockdown efficiency using specific antibodies against PLK1, LKB1, CAMKKβ, and tubulin, related to Figures 2D and S2E. The shLKB1-#1 was selected to deplete endogenous LKB1. **G**, The reduced AMPK activity caused by PLK1 inhibition or/and CDK1 inhibition in mitosis was restored under starvation. U2OS cells were synchronized in mitosis with nocodazole block (16 h). Then, cells were treated with starvation medium (HBSS) for 1 h, in the presence of PLK1 inhibitor BI2536 or/and Cdk inhibitor roscovitine, and MG132. AMPK activity was analyzed by Western blotting with pT172-AMPK. Nocodazole, 100 ng/ml. BI2536, 100 nM. Roscovitine, 50 μM. MG132, 10 μM. **H**, The average +/- SEM of each panel as in Figure 2F.

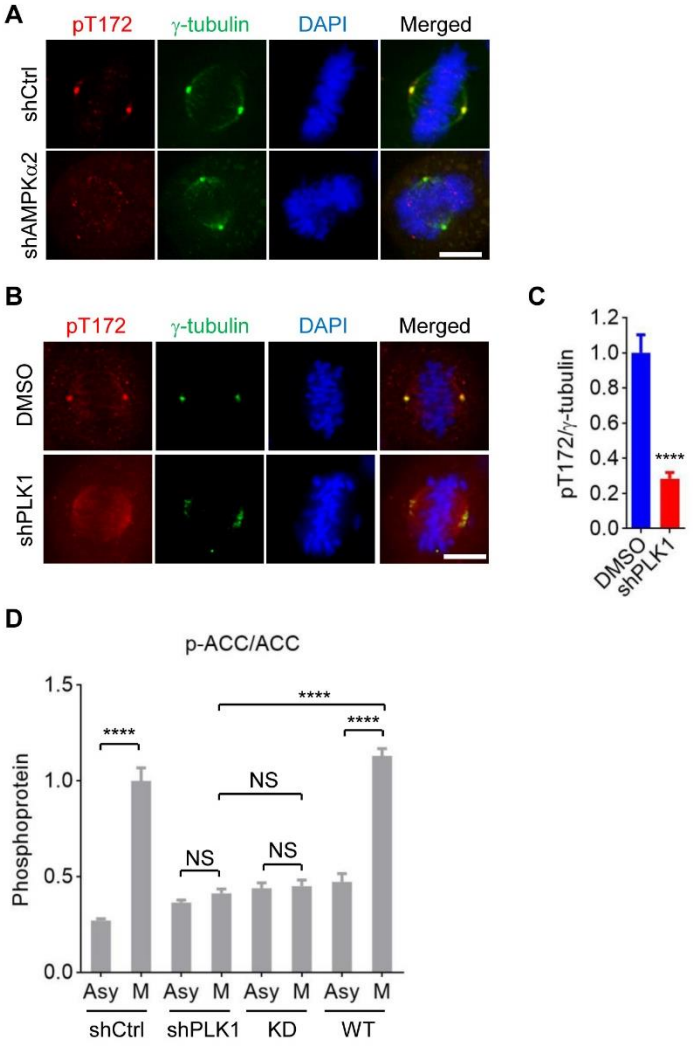

Figure S3. PLK1 regulates mitotic AMPKα2 activity (related to Figure 3)

A, The pT172 signal is abolished in cells depleted of AMPKα2. HeLa cells stably expressing shAMPKα2 were treated with double thymidine block followed by releasing for 8 h. Cells were fixed, permeabilized, and stained for pT172 (red), γ-tubulin (green), and DAPI (blue). γ-tubulin, centrosomal marker. Scale bar, 10 μm. **B**, Immunostaining of active form AMPKα2 in PLK1-depleted cells. HeLa cells stably expressing PLK1 shRNA were treated with double thymidine block. Cells were fixed and stained for pT172 (red), γ-tubulin (green), and DAPI (blue). Scale bar, 10 μm. **C**, Quantification of immunofluorescence intensity in (B). Data represent mean ± SEM. The experiment was repeated three times independently. Statistical significance was determined by unpaired two-tailed t-test. ****p<0.0001. The average +/- SEM of each pane was 1.000 ± 0.1039, 0.2850 ± 0.03378. **D**, Quantification of pS79-ACC levels as in Figure 3H. Ordinary one-way ANOVA followed by Tukey's multiple comparisons test was used to determine statistical significance. NS (not significant) indicates p>0.05. ****p<0.0001. The average +/- SEM of each panel was 0.2710 ± 0.008775, 1.000 ± 0.06764, 0.3646 ± 0.01270, 0.4122 ± 0.02265, 0.4388 ± 0.02903, 0.4497 ± 0.03192, 0.4732 ± 0.04268, 1.131 ± 0.03685.

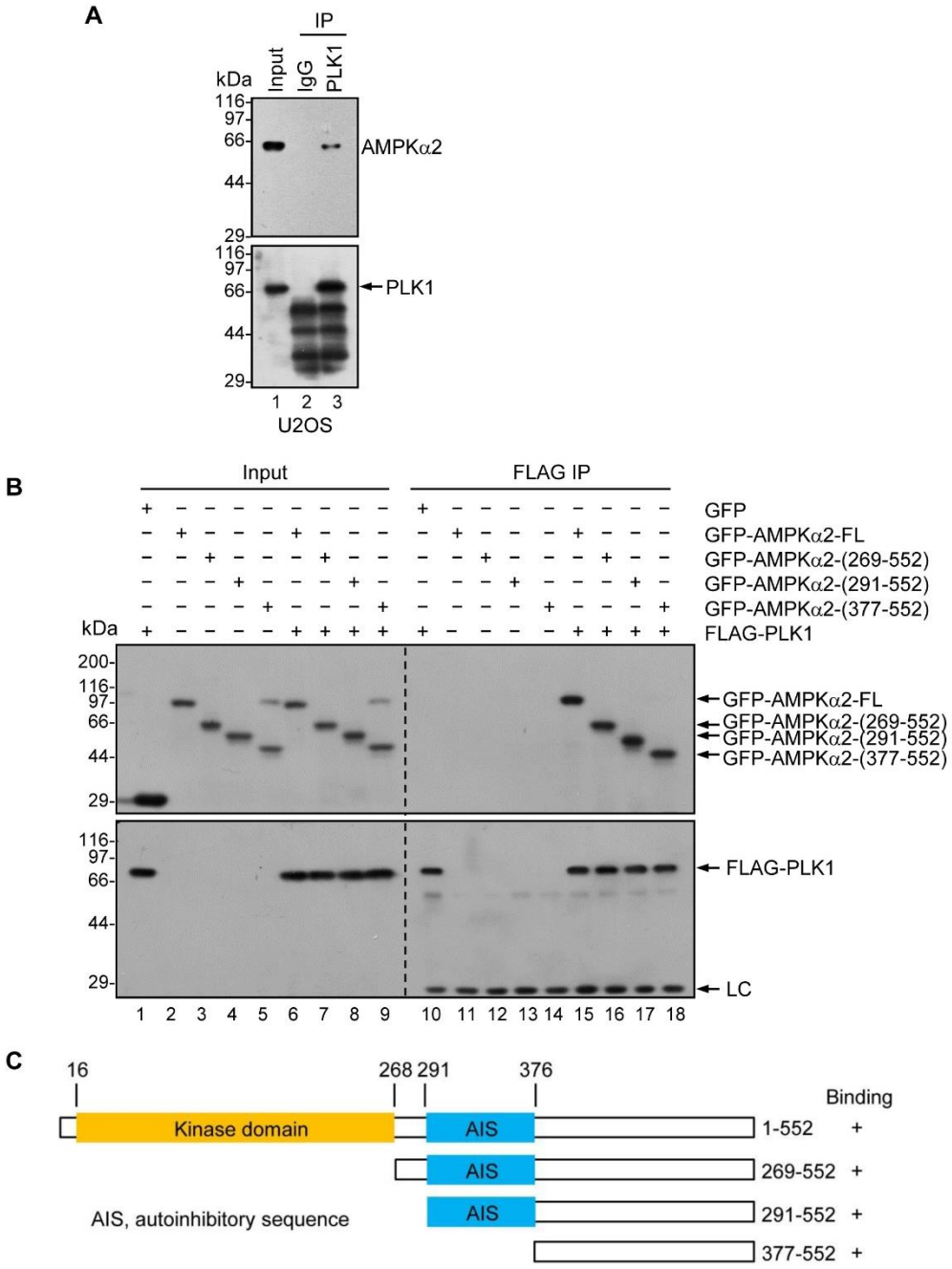

Figure S4. PLK1 binds specifically to AMPKα2 via the PBD domain (related to Figure 4)

A, Co-immunoprecipitation of PLK1 and AMPKα2. Lysates of U2OS cells were subjected to immunoprecipitation by using an antibody against PLK1. Then the precipitates were examined by immunoblotting with the anti-AMPKα2 antibody. **B**, Co-immunoprecipitation of FLAG-PLK1 and GFP-tagged AMPKα2 or AMPKα2 truncation. HEK293T cells were transfected with FLAG-PLK1 and GFP-AMPKα2 (full length, or the truncated mutants). Cell lysates were incubated and immunoprecipitated with anti-FLAG antibody. The bound GFP-AMPKα2 was immunoblotted as indicated. **C**, A summary of the association between PLK1 and AMPKα2 containing the indicated C-terminal truncations, related to Figure S4B.

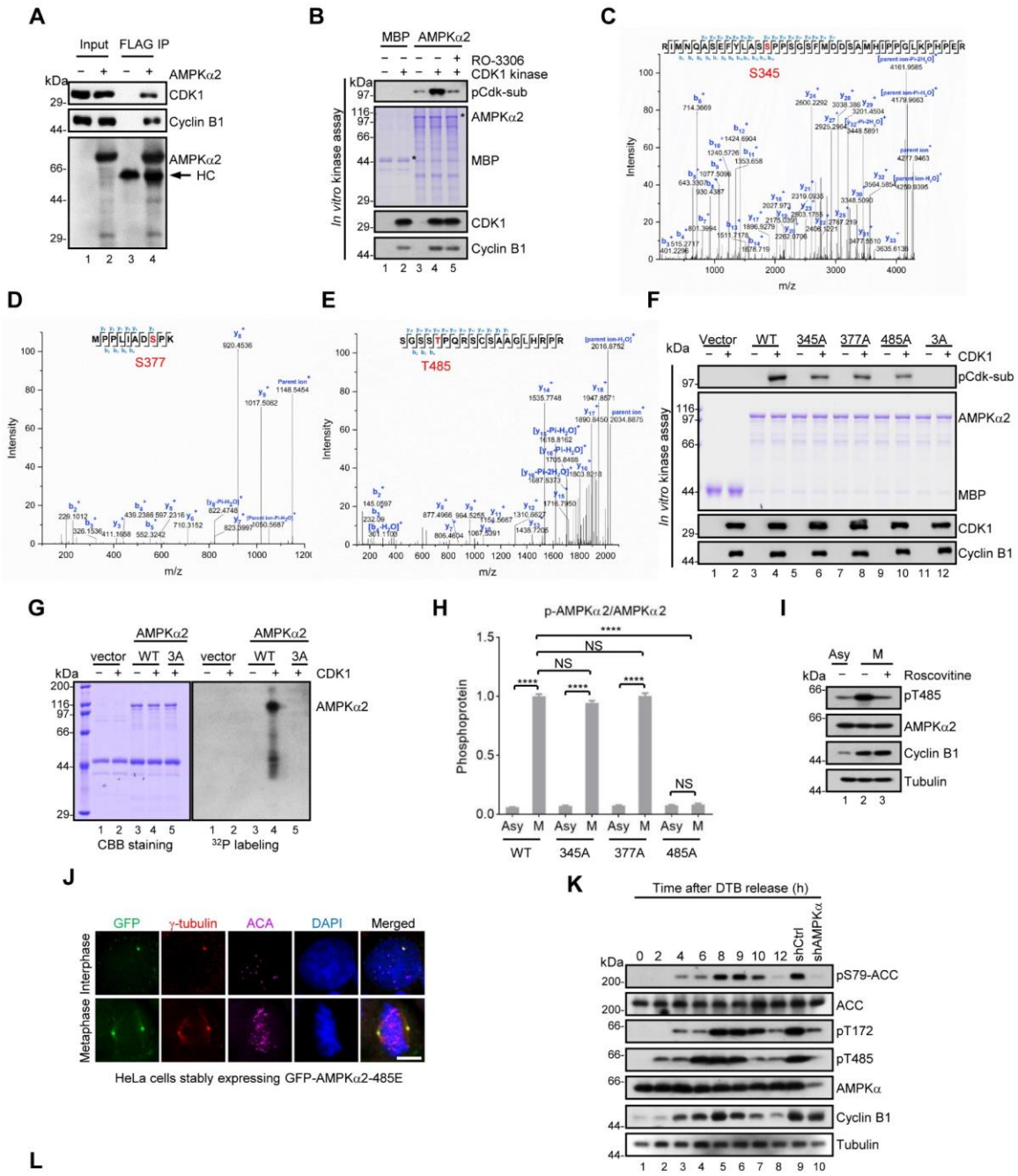

L

	WT+DMSO	WT+Roscovitine	WT+BI2536	485E+DMSO	485E+Roscovitine
K_m (μM)	5.225±1.476	6.921±2.275	6.986±2.759	3.828±0.6670	3.752±0.8740
k_{cat} (min^{-1})	9.429±0.8297	4.730±0.5438	3.258±0.4517	12.47±0.5998	11.60±0.7400
k_{cat}/K_m ($\mu M^{-1} \cdot min^{-1}$)	1.805	0.683	0.466	3.258	3.092

Figure S5. Phosphorylation and activation of AMPKα2 by PLK1 depends on Thr485 priming phosphorylation (related to Figure 5)

A, Co-immunoprecipitation of FLAG-AMPKα2 and endogenous CDK1-Cyclin B1 complex. HeLa cells were transfected with FLAG-AMPKα2 and were synchronized in mitosis by treatment with 100

ng/ml nocodazole for 16 h. Cell lysates were subjected to immunoprecipitation with anti-FLAG and subsequently immunoblotted as indicated. **B**, *In vitro* kinase assay using recombinant CDK1-Cyclin B1 complex and purified MBP-AMPKα2. The phosphorylation level of AMPKα2 was analyzed by immunoblotting with the indicated antibodies. The pCdk-sub, a specific antibody recognizing phosphorylated substrates of CDK kinase. **C**-**E**, Mass spectrometry of AMPKα2 phosphorylation. **F**, *In vitro* kinase assay using recombinant CDK1-Cyclin B1 complex and purified MBP-AMPKα2, MBP-AMPKα2-345A, MBP-AMPKα2-377A, MBP-AMPKα2-485A, or MBP-AMPKα2 3A mutant. Samples were immunoblotted with the indicated antibodies. 3A mutant, Ser345, Ser377, and Thr485 were all replaced by Ala. **G**, *In vitro* kinase assay using recombinant CDK1-Cyclin B1 complex and purified MBP-tagged AMPKα2 or 3A mutant. The phosphorylation level of AMPKα2 or 3A mutant was analyzed by using ^{32}P-labeled ATP. 3A mutant, Ser345, Ser377, and Thr485 were all replaced by Ala. **H**, Quantification of pT172-AMPKα2 levels as in Figure 5B. Data represent mean ± SEM. The experiment was repeated three times independently. Ordinary one-way ANOVA followed by Tukey's multiple comparisons test was used to determine statistical significance. NS (not significant) indicates p>0.05. ****p<0.0001. The average +/- SEM of each panel was 0.06060 ± 0.001755, 1.000 ± 0.01771, 0.07185 ± 0.003262, 0.9444 ± 0.01913, 0.07520 ± 0.003126, 1.004 ± 0.02379, 0.07667 ± 0.004339, 0.08347 ± 0.009988. **I**, The phosphorylation level of AMPKα2 at Thr485 in mitotic cells. Nocodazole-arrested (100 ng/ml, for 16 h) mitotic HeLa cells were treated with 50 μM roscovitine in the presence of 10 μM MG132 for 1 h. Whole-cell lysates (WCL) were separated by SDS-PAGE and immunoblotted with the anti-phospho-Thr485 antibody. Asy, asynchronous. M, mitotic. **J**, AMPKα2-485E mutant localizes on centrosomes. HeLa cells stably expressing GFP-AMPKα2-485E mutant were treated with double thymidine block (2.5 mM thymidine, 16 h each time) followed by releasing for 8 h. Cells were fixed, permeabilized, and stained for γ-tubulin (red), ACA (magenta), and DAPI (blue). Scale bar, 10 μm. **K**, HeLa cells were synchronized at the G1/S boundary by double thymidine block (DTB, 16 h each time) and released to the indicated time points. Samples were analyzed with depicted antibodies. HeLa cells stably expressing shRNA control and AMPKα shRNA arrested in mitosis with nocodazole (Noc, 100 ng/ml) treatment were used as controls. Thymidine, 2.5 mM. **L**, The enzyme kinetics of AMPKα2 (WT or the 485E mutant) were calculated according to the Michaelis-Menten equation in the conditions indicated, related to Figure 5I.

A

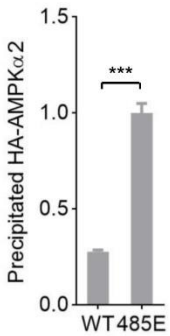

Figure S6. Thr485 phosphorylation promotes the binding of PLK1 to AMPKα2 (related to Figure 6)

A, Quantification of precipitated HA-AMPKα2 as in Figure 6E. Data represent mean ± SEM. The experiment was repeated three times independently. Statistical significance was determined by unpaired two-tailed t-test. ***p=0.0001. The average +/- SEM of each pane was 0.2757 ± 0.009999, 1.000 ± 0.04849.

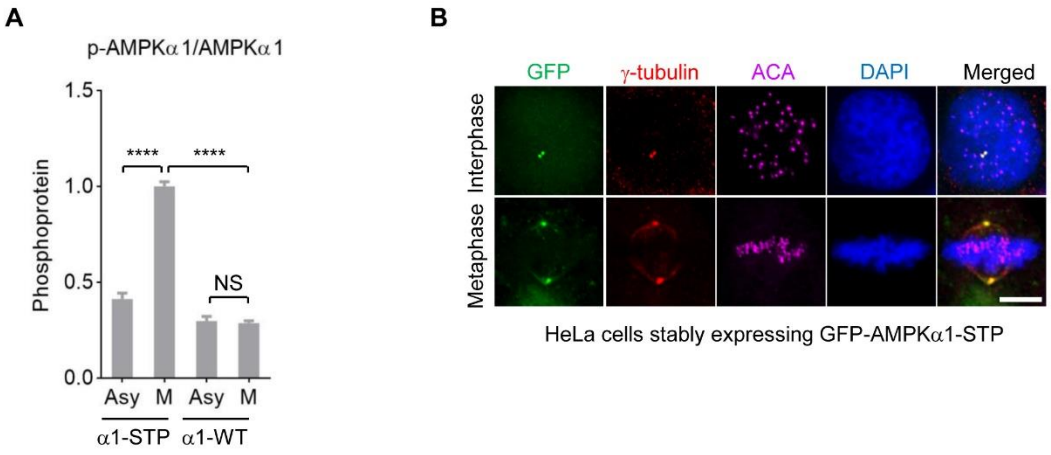

Figure S7. AMPKα1-STP mutant localizes on centrosomes (related to Figure 7)

A, Quantification of pT172-AMPKα1 as in Figure 7F. Data represent mean ± SEM. The experiment was repeated three times independently. Ordinary one-way ANOVA followed by Tukey's multiple comparisons test was used to determine statistical significance. NS (not significant) indicates $p>0.05$. ****$p<0.0001$. The average +/- SEM of each pane was 0.4122 ± 0.03138, 1.000 ± 0.02532, 0.2975 ± 0.02360, 0.2871 ± 0.01185. **B**, HeLa cells stably expressing GFP-AMPKα1-STP mutant were treated with double thymidine block (2.5 mM thymidine, 16 h each time) followed by releasing for 8 h. Cells were fixed, permeabilized, and stained for γ-tubulin (red), ACA (magenta), and DAPI (blue). Scale bar, 10 μm.

TRANSPARENT METHODS

Plasmid Constructs

FLAG-AMPKα1, FLAG-AMPKα2, FLAG-PLK1, and HA-AMPKα2 were generated by cloning the cDNA of AMPKα1, AMPKα2, or PLK1 into corresponding p3×FLAG-CMV-24 or pcDNA3-3×HA expression vector with ClonExpress II (Vazyme) (Mo et al., 2016). MBP-AMPKα1 and MBP-AMPKα2 were made by subcloning cDNA from the respective p3×FLAG-CMV-24 vector into the pMal-c2 vector. The GST-tagged plasmids expressing PLK1 and its fragments were generated by subcloning cDNA from the corresponding p3×FLAG-CMV-24 into the pGEX-6P vector (Xia et al., 2012). Site-directed mutagenesis was performed using Mut Express II (Vazyme) according to the manufacturer's instructions. Mammalian co-expression plasmid FLAG-CDK1-Cyclin B1 was generated by inserting 3xFLAG-CDK1 from respective p3×FLAG-CMV-24 vector into the MCS of pIRES2-ZsGreen1 vector and replacing the ZsGreen1 coding frame with Cyclin B1. All plasmids used were verified by sequencing (Invitrogen).

Antibodies

Anti-HA-tag (3724, 1:2,000), anti-pS10-H3 (3377, 1:5,000), anti-AMPKα (5831, 1:1,000), anti-AMPKα2 (2757, 1:1,000), anti-phospho-AMPK-Thr172 (2535, 1:1,000), anti-ACC (3662, 1:1,000), anti-phospho-ACC-Ser79 (11818, 1:1,000), anti-phospho-PLK1-Thr210 (9062, 1:1,000), anti-Cyclin B1 (4135, 1:1,000), anti-CDK1 (77055, 1:1,000), anti-phospho-CDK-substrates (9391, 1:1,000) and anti-CAMKKβ (16810, 1:1,1000) antibodies were from Cell Signaling Technology. Anti-AMPKα1 (ab32047, 1:1,000) and anti-α-tubulin (ab80779, 1:5,000) were from Abcam. Anti-PLK1 (sc-17783, 1:1,000), anti-γ Tubulin (sc-17787, 1:50) and anti-LKB1 (sc-32245, 1:1,000) were from Santa Cruz. Anti-FLAG-tag (F3165, 1:2,000) and anti-GFP-tag (G6539, 1:2,000) were from Sigma Aldrich. Anti-BUBR1 (612502, 1:2,000) was from BD Biosciences. Anti-pS676-BUBR1 (1:2,000) was a kind gift from E. A. Nigg, University of Basel, Switzerland. Anti-pT485-AMPKα2 (1:1,000) antibody was generated by YenZym LLC. To generate anti-pT485-AMPKα2 antibody, a synthetic peptide containing phosphorylated T485 (VEQRSGSS-pT-PQRSCS) was conjugated to rabbit albumin (Sigma) and injected into rabbits as previously described (Yao et al., 1997). Serum was collected by a standard protocol and preabsorbed by unphosphorylated AMPK peptide (VEQRSGSSTPQRSCS) followed by affinity-purification using (VEQRSGSS-pT-PQRSCS)-conjugated divinylsulfone Sepharose beads as previously reported (Mo et al., 2016). Secondary antibodies were from Jackson ImmunoResearch Laboratory.

Reagents

Reversine (1 μM), Hesperadin (25 nM), Nocodazole (100 ng/ml), MG132 (10 μM), Roscovitine (50 μM), and RO-3306 (9 μM) were from Sigma. BI2536 (100 nM) was from Selleck Chemicals. Calf Intestinal alkaline phosphatase (CIP) was purchased from New England BioLabs. The protease inhibitors cocktail was from Sigma and phosphatase inhibitors were from Roche.

Cell Culture and Synchronization

HEK293T, U2OS, and HeLa cells were purchased from the American Type Culture Collection and

maintained as monolayers in advanced DMEM (Invitrogen) with 10% FBS (HyClone) and 100 units/mL of penicillin plus 100 μg/mL of streptomycin (Invitrogen). The cell lines used were not found in the International Cell Line Authentication Committee (ICLAC) listings for cross-contaminated or otherwise misidentified cell lines. The cells were routinely tested for mycoplasma contamination. For cell cycle synchronization, HeLa or U2OS cells were first blocked in G1/S with 2.5 mM thymidine (Sigma) for 16 h and then released in fresh culture medium for 8 h to enrich mitotic cells. Plasmid transfections were performed with Lipofectamine 2000 (Invitrogen) according to the manufacturer's instructions.

Lentivirus-Based RNA Interference and Protein Expression

The vector pLKO.1 along with psPAX2 and pMD.2G were used for producing shRNA-packaged viral particles as previously described (Mo et al., 2016). The nucleotide sequences inserted into pLKO.1 for gene depletion were listed:

LKB1: 5'- CCGGaacgaagagaagcagaaaatgCTCGAGcattttctgcttctcttcgttTTTTTG-3' (#1)
and 5'-CCGGgggtcaccctctacaacatcaCTCGAGtgatgttgtagagggtgacccTTTTTG-3' (#2)
AMPKα1: 5'-CCGGgaggagagctatttgattataCTCGAGtataatcaaatagctctcctcTTTTTG-3'
AMPKα2: 5'-CCGGgagagcatgaatggtttaaacCTCGAGgtttaaaccattcatgctctcTTTTTG-3'
AMPKα1α2: 5'-CCGG atgatgtcagatggtgaatttCTCGAGaaattcaccatctgacatcatTTTTTG-3'
CAMKKβ: 5'-CCGGgtgtgcagctgaatcagtataCTCGAGtatactgattcagctgcacacTTTTTG-3'
PLK1: 5'-CCGGagattgtgcctaagtctctgcCTCGAGgcagagacttaggcacaatctTTTTTG-3'.

For stable expression, pLKO.1 along with psPAX2 and pMD.2G were transfected into HEK293T cells with Lipofectamine 2000 reagent (Invitrogen) according to the manufacturer's instructions. Forty-eight hours after transfection, the supernatant was collected and added to HeLa or U2OS cells. Thirty-six hours after infection, cells were selected with puromycin (2 μg/mL) for two weeks.

For protein expression, the cDNA of AMPK or PLK1 was subcloned into lentivirus-based vector pLVX-GFP or pLVX-FLAG. The constructed plasmid along with psPAX2 and pMD.2G were transfected into HEK293T cells with Lipofectamine 2000 reagent. Forty-eight hours after transfection, the medium was collected and added to the target cell. For screening stable cell lines, cells were selected with puromycin (2 μg/mL) at 36 h after infection for 2 weeks.

For rescue/add back experiments, the RNAi-resistant gene of AMPKα2 or PLK1 was subcloned into lentivirus-based vector pLVX-FLAG. The constructed plasmid along with psPAX2 and pMD.2G were transfected into HEK293T cells with Lipofectamine 2000 reagent. Forty-eight hours after transfection, the medium was collected and added to the shRNA stable cell line.

Recombinant Protein Purification

GST-PLK1, GST-PLK1-N, GST-PLK1-C, GST-PBD, GST-PBD-2A, MBP-AMPKα1, MBP-AMPKα1-mutant (T490A/T490E), MBP-AMPKα2, and MBP-AMPKα2 (T485A/T485E) were produced from bacteria as previously described (Xia et al., 2012). The plasmids were transformed into the *E. coli* strain Rosetta (DE3), and protein expression was induced with 0.2 mM IPTG at 16°C for 16 h. To purify GST-tagged protein, the cells that carried encoding protein were harvested by centrifugation and the pellets were suspended in PBS supplemented with 10 mM β-mercaptoethanol and 0.1 mM

phenylmethylsulfonyl fluoride (PMSF) and incubated on ice for 30 min. After sonication, the cell lysates were centrifuged at 13,000×g for 20 min. The supernatants were mixed with GST agarose resin (GE Healthcare Life Science) and rotated at 4°C for 1 h. The resins were subjected to three successive washes with PBS, and proteins were released from resins with 10 mM glutathione. For MBP-tagged protein purification, the cells were suspended in MBP column buffer (20 mM Tris-HCl, pH 7.4, 200 mM NaCl, and 1 mM EDTA). After sonication, the supernatants were mixed with amylose resin (New England BioLabs) at 4°C for 1 h. The resins were washed three times in MBP column buffer, and proteins were eluted from the resin with MBP column buffer containing 10 mM maltose. All purification procedures were performed at 4°C, in the presence of protease inhibitor cocktail (Sigma).

Western Blotting

Proteins from lysed cells were subjected to SDS/PAGE and transferred onto nitrocellulose membranes. After blocking with 5% (W/V) bovine serum albumin, the membrane was probed by the indicated primary and secondary antibodies and detected using ECL.

Immunoprecipitation and Pull-Down Assays

For immunoprecipitation, cells were treated with the indicated reagents before being lysed in lysis buffer (50 mM Tris-HCl, pH 7.5, 120 mM NaCl, 0.2% NP-40, 1 mM EDTA, and 1 mM DTT) supplemented with protease inhibitor cocktail (Sigma) and phosphatase inhibitor cocktail (Sigma). After pre-clearing with protein A/G resins, the lysate was incubated with the indicated antibody at 4°C for 24 h with gentle rotation. Protein A/G resins were then added to the lysates and incubated at 4°C for 4 h. The resins were spun down and washed four times with lysis buffer before being resolved by SDS-PAGE and immunoblotted with the indicated antibodies. For FLAG-tagged protein immunoprecipitation, the FLAG-M2 resin was added to the lysates and incubated for 4 h before washing. For *in vitro* reactions, the FLAG beads were further washed twice with dialysis buffer, and the FLAG-tagged protein was eluted with dialysis buffer supplemented with 100 μg/mL FLAG peptide (Sigma). For pull-down assays, GST or GST-tagged proteins purified from bacteria were incubated with the cell lysates for 4 h, after which the bound fraction was washed with lysis buffer four times and analyzed by Western blotting.

***In Vitro* Kinase Assay**

The kinase reactions were performed in 40 μL kinase buffer (25 mM HEPES, pH 7.2, 50 mM NaCl, 2 mM EGTA, 5 mM $MgSO_4$, 1 mM DTT, and 0.01% Brij35) with purified AMPK (2 μg) as substrate, 100 ng CDK1 (NEB) or PLK1 (Abcam) kinase, 50 μM ATP with or without 5 μCi of [γ-^{32}P]-ATP and as described previously (Mo et al., 2016). Reaction mixtures were incubated at 30°C for 30 min, then terminated by 5×SDS-PAGE loading buffer (10% SDS, 0.5% bromophenol blue, 50% glycerol, and 100mM DTT). After the samples were boiled at 100°C for 2 min, 50% of the sample was resolved by SDS-PAGE. For the reaction without [γ-^{32}P]-ATP, samples were subjected to Western blotting with the indicated antibodies to test the phosphorylation levels. For the reaction in the presence of [γ-^{32}P]-ATP, samples were stained by coomassie brilliant blue R250 (CBB). For

autoradiograms, CBB-stained SDS-PAGE gels were de-stained, scanned, and then dried between sheets of cellulose for 4 h. The semi-dried gels were then placed between intensifier and X-ray films for 12-24 h in a −80°C freezer, to determine the levels of ^{32}P incorporation into AMPK proteins.

Immunofluorescence and Time-Lapse Imaging

HeLa or U2OS cells grown on coverslips were fixed by a pre-extraction method using PTEM buffer (60 mM PIPES, pH 6.8, 10 mM EGTA, 2 mM $MgCl_2$, and 0.1% Triton X-100) supplemented with 3.7% paraformaldehyde. After blocking with PBST (PBS with 0.05% Tween-20) buffer containing 1% bovine serum albumin (Sigma) for 45 min at room temperature, the fixed cells were incubated with primary antibodies in a humidified chamber for 1 h at room temperature or overnight at 4°C, followed by secondary antibodies for 1 h at 37°C. The DNA was stained with DAPI from Sigma. Images were captured by Delta Vision softWoRx software (Applied Precision) and processed by deconvolution and z-stack projection. For Time-lapse imaging, HeLa cells were cultured in glass-bottom culture dishes (MatTek) and maintained in CO_2-independent media (Gibco) supplemented with 10% FBS and 2 mM glutamine. During imaging, the dishes were placed in a sealed chamber at 37°C. Images of living cells were taken with the DeltaVision microscopy system.

AMPK Kinetics Assay

The kinetics of AMPK was characterized by the Amplite™ Universal Fluorimetric Kinase Assay Kit (AAT Bioquest) according to the manufacturer's instructions. In brief, 200 nM eluted FLAG-AMPKα2 (wild-type and mutants) were incubated with gradient concentrations of SAMS in 20 μL kinase reaction buffer (ADP assay buffer) at 37°C for 30 min; 20 μL ADP sensor buffer and 10 μL ADP sensor were added into the preparations to make a total 50 μL ADP assay volume. The reaction mixture was incubated at room temperature for 30 min. The amount of ADP produced from the kinase reaction assay was detected by monitoring the fluorescence intensity at Ex/Em=540/590 nm. The background fluorescence was determined by measuring the fluorescence intensity in the absence of substrate and subtracted from the experiments. K_m and k_{cat} values were calculated by the Michaelis-Menten equation as previously reported (Huang et al., 2019).

Fluorescence Intensity Quantification

Quantification of fluorescence intensity of centrosome-associated proteins was performed as described previously using Image J (Mo et al., 2016). In brief, the average pixel intensities from no less than five cells (which were randomly selected) were measured, and background pixel intensities were subtracted. The pixel intensities at each centrosome pair were then normalized against ACA values to account for any variations in staining or image acquisition.

Statistical Analysis

Statistical analyses were performed using GraphPad Prism 8.0. All data were tested for normality using Shapiro-Wilk and Kolmogorov-Smirnov tests. If passed, an unpaired two-tailed Student's *t*-test was used to compare two groups or one-way ANOVA followed by Tukey's post-hoc test for comparisons among >2 groups. Otherwise, nonparametric tests (Mann-Whitney U test or Kruskal-

Wallis test followed by Dunn's post-hoc test) were used. *P* value <0.05 was considered statistically significant. Data are presented as means ± SEM. Statistics tests used are indicated in the corresponding figure legends. Experiments were repeated three independent times.

Supplemental References

Huang, Y., Lin, L., Liu, X., Ye, S., Yao, P.Y., Wang, W., Yang, F., Gao, X., Li, J., and Zhang, Y*., et al.* (2019). BubR1 phosphorylates CENP-E as a switch enabling the transition from lateral association to end-on capture of spindle microtubules. CELL RES *29*, 562-578.

Mo, F., Zhuang, X., Liu, X., Yao, P.Y., Qin, B., Su, Z., Zang, J., Wang, Z., Zhang, J., and Dou, Z*., et al.* (2016). Acetylation of Aurora B by TIP60 ensures accurate chromosomal segregation. NAT CHEM BIOL *12*, 226-232.

Xia, P., Wang, Z., Liu, X., Wu, B., Wang, J., Ward, T., Zhang, L., Ding, X., Gibbons, G., and Shi, Y*., et al.* (2012). EB1 acetylation by P300/CBP-associated factor (PCAF) ensures accurate kinetochore-microtubule interactions in mitosis. Proc Natl Acad Sci U S A *109*, 16564-16569.

Yao, X., Anderson, K.L., and Cleveland, D.W. (1997). The microtubule-dependent motor centromere-associated protein E (CENP-E) is an integral component of kinetochore corona fibers that link centromeres to spindle microtubules. J CELL BIOL *139*, 435-447.